ASIA-AQ/SIJAQ

Rapid Science Synthesis Report

National Institute of
Environmental Research

ASIA-AQ/SIJAQ Rapid Science Synthesis Report

Co-authors: Rokjin Park[1], Jhoon Kim[2], Meehye Lee[3], Taehyung Lee[4], Ukkyo Jeong[5], Jaein Jeong[1], Gang-Woong Lee[4], Jung-Hun Woo[1], Chang-Keun Song[6], Cheol-Hee Kim[7], Soontae Kim[8], Mijung Song[9], Hanlim Lee[5], Changsub Shim[10], Sung-Kyun Shin[11], Jiwon Seong[12], Jungmin Park[12], Jae-Bum Lee[12], Hye Jung Shin[12], Lim-seok Chang[12], Joon Young Ahn[12], Jin Soo Park[12], Suna Shin[12], Soi Ahn[12], Hyunkee Hong[12]

[1]Seoul National University, Seoul, KR
[2]Yonsei University, Seoul, KR
[3]Korea University, Seoul, KR
[4]Hankuk University of Foreign Studies, Seoul, KR
[5]Pukyong National University, Pusan, KR
[6]Ulsan National Institute of Science and Technology, Ulsan, KR
[7]Jeonbuk National University, Jeonju, KR
[8]Pusan National University, Busan, KR
[9]Ajou University, Suwon, KR
[10]Korea Environment Institute, Sejong, KR
[11]The Seoul Institute, Seoul, KR
[12]National Institute of Environmental Research, Incheon, KR

Consultants: Yong-Pyo Kim[1], Seog-Yeon Cho[2], Myoung-Hwan Ahn[3]

[1]Seoul National University, Seoul, KR
[2]Inha University, Incheon, KR
[3]Ewha Womans University, Seoul, KR

Reviewers: James. H. Crawford[1], Jack E. Dibb[2], Pedro Campuzano-Jost[3], Isobel Simpson[4], Katherine Travis[1], and Greg Carmichael[5]

[1]Langley Research Center, NASA, USA
[2]Earth Systems Research Center, University of New Hampshire, USA
[3]University of Colorado Boulder, USA
[4]University of California, Irvine, USA
[5] University of Iowa, Iowa City, USA

Contents

Summary of Campaign Findings for Policy Makers

- **Drivers of Korea's wintertime air quality: ASIA-AQ Insights**

Since the Korea–United States Air Quality (KORUS-AQ) joint campaign in 2016, there have been notable changes in anthropogenic pollutant emissions across East Asia, including the Korean Peninsula. In the period spanning February to March of 2024, the nationwide average concentration of $PM_{2.5}$ in South Korea was recorded at 19.9 μg m^{-3}, indicating a ~31% decrease compared to the average of 28.6 μg m^{-3} observed during the same months from 2015 to 2023 during which a significant interannual variability of annual mean $PM_{2.5}$ concentrations was observed. A scientific investigation was conducted to examine the factors and mechanisms contributing to the recent decrease in $PM_{2.5}$ concentrations and the sporadic occurrences of elevated wintertime pollution events. This investigation was carried out by the National Institute of Environmental Research (NIER, KOREA) and the National Aeronautics and Space Administration (NASA, USA) in collaboration, with the ASIA-AQ/SIJAQ (IV) observation campaign being implemented over a two-month period from February to March 2024. A comprehensive evaluation of surface, airborne, satellite, and modeling data collected during the campaign was conducted to ascertain the primary findings and recommendations concerning $PM_{2.5}$ pollution in South Korea.

- **Strategy for winter $PM_{2.5}$: Limit HNO_3 formation and Nitrate loads**

A comprehensive analysis of ground-based and airborne observations conducted during the campaign period revealed that wintertime $PM_{2.5}$ pollution in South Korea was predominantly secondary in origin. Among the chemical components, nitrate concentrations exhibited the greatest increase during episodes of elevated $PM_{2.5}$. To effectively reduce wintertime $PM_{2.5}$ concentrations, it is essential to target reductions in inorganic nitrate, which is the dominant contributor. Inorganic nitrate is predominantly formed from nitric acid (HNO_3), which is produced through the reaction of nitrogen dioxide (NO_2) with hydroxyl radicals (OH) in the atmosphere. Consequently, endeavors aimed at reducing HNO_3 should not be limited to the mitigation of nitrogen oxide (NOx) emissions. These efforts should also acknowledge the regulation of ozone levels, given the impact on OH production, as well as the management of emissions from volatile organic compounds (VOCs), which also influence radical chemistry.

- **Beyond Nitrate: Aromatics-origin SOA Control for Winter $PM_{2.5}$ and Ozone in summer**

Despite the relatively minor contribution (20%) of organic aerosols (OA) to wintertime high-$PM_{2.5}$ episodes, sustained reductions in $PM_{2.5}$ concentrations necessitate targeted mitigation of OA, particularly secondary organic aerosol (SOA). Toluene has been identified as a significant contributor to SOA formation, maintaining its position as a reliable indicator, as evidenced by the findings of the KORUS-AQ study conducted in 2016. Consequently, the sustained management of toluene and associated emission sources is imperative to achieve co-benefits in reducing both summertime ozone and wintertime $PM_{2.5}$ pollution.

- **Favorable winter synoptics and emission cuts lower Korea's $PM_{2.5}$**

During the campaign, the relative contributions of external and domestic sources to $PM_{2.5}$ concentrations in South Korea ranged from 57% to 84% and from 16% to 43%, respectively. The magnitude of these contributions exhibited considerable variability, contingent upon the synoptic meteorological conditions that prevailed over the Korean Peninsula. In particular, the synoptic weather pattern that dominated the region during the winter of 2024 played a pivotal role in determining the concentrations of $PM_{2.5}$. Accordingly, the observed decrease in wintertime $PM_{2.5}$ concentrations in 2024, relative to the 2015–2023 period, was likely driven not only by reductions in anthropogenic emissions across East Asia (including South Korea) but also by favorable meteorological conditions associated with the El Niño event.

- **Upgrading Korea's AQ models with meteorology, upwind emissions, and GEMS**

A comparison of observational data and model outputs during the ASIA-AQ campaign demonstrated the satisfactory performance of domestic chemical transport models in predicting air quality and informing environmental policy. Nevertheless, the accuracy of model simulations can be further enhanced by improving key input datasets, particularly meteorological fields and upwind emissions inventories. Continued use of high-quality satellite observations, such as those from the Geostationary Environment Monitoring Spectrometer (GEMS), is expected to significantly improve model performance in the future.

1. Introduction

East Asia has undergone substantial changes since the Korea–United States Air Quality (KORUS-AQ) campaign, which was conducted from May to June of 2016 and focused on investigating air quality over the Korean Peninsula. China has implemented a series of stringent air quality policies aimed at reducing anthropogenic emissions, while South Korea has introduced enhanced air quality management measures, including the seasonal management program. Moreover, the region underwent a period of accelerated and extensive socio-economic upheaval as a result of the pandemic. These developments are presumed to have significantly altered anthropogenic pollutant emissions across East Asia. In order to better understand the impact of these alterations on wintertime fine particulate pollution over the Korean Peninsula, the National Institute of Environmental Research (NIER, KOREA) and the National Aeronautics and Space Administration (NASA, USA) collaboratively executed the ASIA-AQ/SIJAQ (IV) observation campaign during February–March 2024. The primary objective of this study was to scientifically investigate and understand the causes and processes underlying air pollution driven by particulate matter in South Korea, with a particular focus on wintertime air quality degradation.

To support this field investigation, comprehensive observations were conducted using ground-based supersites and aircraft platforms. These included two Korean aircraft (King Air 1900D and King Air C90GT), NASA's DC-8 and G-III aircraft, and the King Air 350HW operated by the Korea Meteorological Administration.

Meteorological Overview During the Campaign Period

The Korean Peninsula during February–March 2024 was strongly influenced by the El Niño event that began in the summer of 2023. Elevated sea surface temperatures across the Indian and Pacific Oceans led to relatively warmer and wetter conditions throughout the campaign period compared with climatological norms. The winter of 2024, which included the campaign months, recorded the highest nationwide precipitation in history and the second warmest winter on record over the Korean Peninsula.

Figure 1 shows the time series of temperature, precipitation, and $PM_{2.5}$ concentrations observed in the capital region during the ASIA-AQ campaign period. The meteorological conditions were characterized by persistent warm southerly marine flow from the Pacific, maintaining above-normal temperatures throughout the campaign period. Mid- to late February (corresponding to P2 in Figure 1) experienced a sharp increase in precipitation that produced sustained clean conditions with lower $PM_{2.5}$ levels. Additional precipitation events in March were accompanied by fluctuating $PM_{2.5}$, reflecting transitional meteorological influences both in the Korean peninsula and upwind source regions (Figure 1).

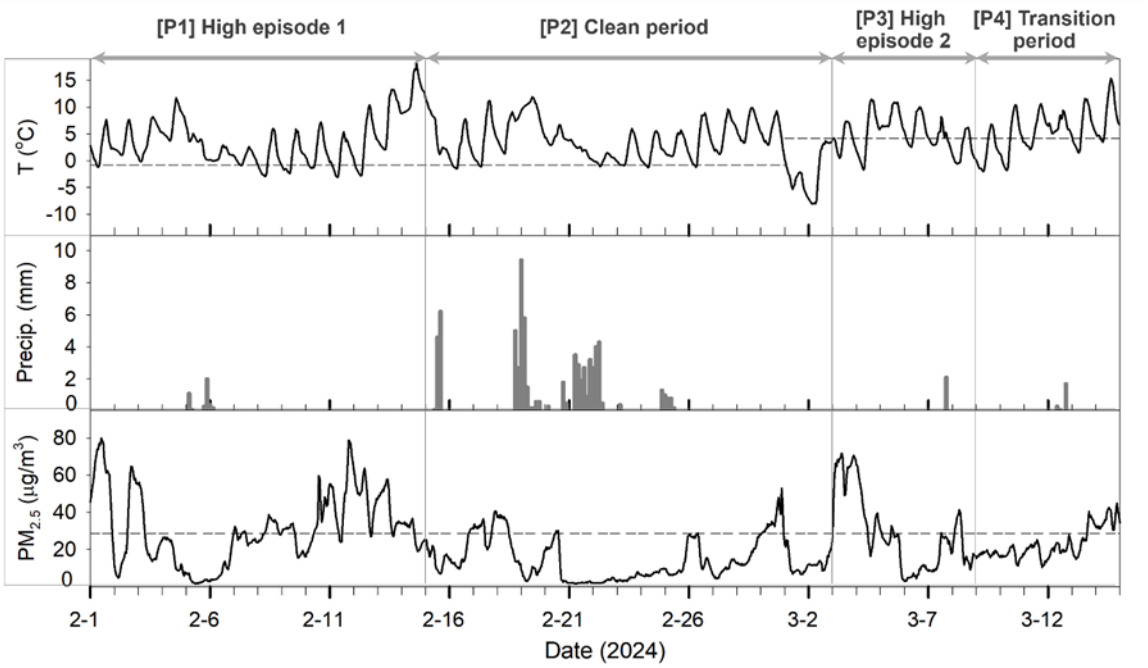

Figure 1. Time series of temperature, precipitation, and $PM_{2.5}$ concentrations observed in the capital region during the ASIA-AQ campaign period. P1–P4 denote the four subperiods used for analysis, defined by $PM_{2.5}$ concentration levels and corresponding meteorological conditions. Dotted lines in the temperature plot denote the climatological mean temperatures for the corresponding periods (1991–2020), and in the $PM_{2.5}$ time series, they indicate the February–March mean concentrations (2015–2023).

The ASIA-AQ campaign period was divided into four subperiod (P1–P4) for analysis based on $PM_{2.5}$ variability and meteorological regimes (Figure 1).

- **P1** (Feb. 1–14): A high-concentration episode under warm conditions with minimal precipitation.
- **P2** (Feb. 15–Mar. 2): A cleaner period dominated by persistent warm and moist inflow with frequent precipitation, effectively lowering $PM_{2.5}$.
- **P3** (Mar. 3–8)**:** A short episode of high $PM_{2.5}$ with intermittent clean intervals.
- **P4** (Mar. 9–15): A transitional phase with relatively lower $PM_{2.5}$ and variable meteorology.

Changes in Wintertime $PM_{2.5}$ Concentrations Over the Korean Peninsula

Long-term statistics of wintertime $PM_{2.5}$ (2015–2024), including the ASIA-AQ campaign window, reveal that 2024 levels were approximately 30–31% lower than the 2015–2023 climatological baseline (Figure 2). The widespread reduction across the Korean Peninsula

reflects the combined influence of (i) continued declines in anthropogenic emissions across East Asia, and (ii) favorable synoptic meteorological anomalies associated with the 2024 El Niño winter.

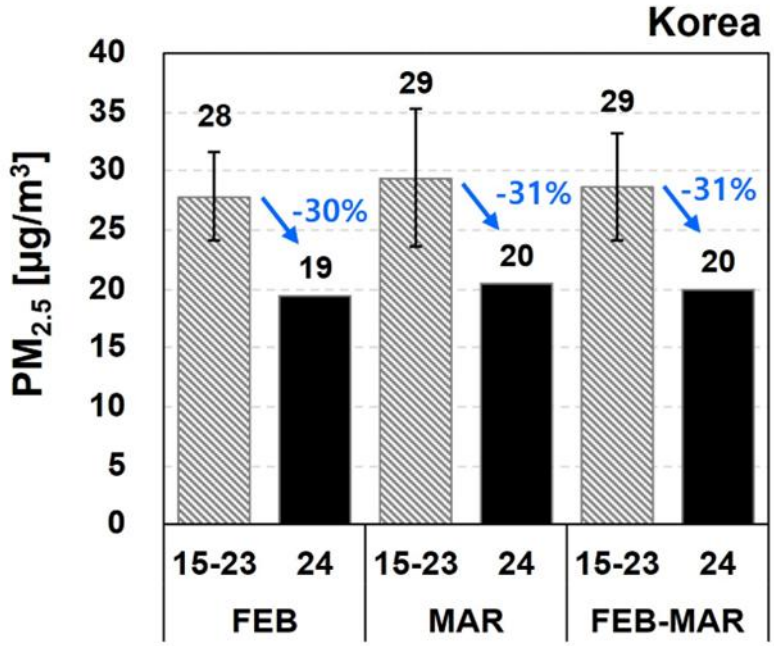

Figure 2. Nationwide $PM_{2.5}$ monthly means for February, March, and February–March, comparing the 2015–2023 climatological average ("15–23") with 2024 ("24"). Vertical bars on the 2015–2023 averages represent ±1σ (one standard deviation) and indicate interannual variability in $PM_{2.5}$ concentrations. Blue labels indicate percent changes in 2024 relative to 2015–2023.

This report provides a comprehensive analysis of $PM_{2.5}$ pollution over the Korean Peninsula based on surface, airborne, and satellite observations, as well as chemical transport modeling during February–March 2024. It characterizes the spatiotemporal distribution, chemical composition, formation mechanisms, and the relative contributions of anthropogenic sources to wintertime $PM_{2.5}$ pollution. Note that the temporal coverage of individual analyses in this report varies depending on data availability and the specific requirements of each methodology. The periods used for each figure and analysis are explicitly noted in the respective figure captions.

2. Questions

This campaign report addresses fundamental scientific inquiries concerning wintertime $PM_{2.5}$ pollution over South Korea, drawing upon the analysis of observational data collected during the ASIA-AQ campaign. While the findings presented here are preliminary, they are supported by a high level of confidence and will be further refined for submission to peer-reviewed scientific journals.

The following inquiries are the primary subjects addressed in this report, along with the scientific background for each:

Q1: Identification of Wintertime $PM_{2.5}$ Formation Mechanisms (What are the dominant chemical mechanisms driving wintertime secondary $PM_{2.5}$ formation in South Korea, and how does nighttime chemistry contribute to this phenomenon?)

Scientific background: Despite the evident decline in solar radiation and the limitation of photochemical activity during winter, South Korea frequently experiences elevated levels of $PM_{2.5}$. These episodes of atmospheric contamination are predominantly driven by the formation of secondary inorganic aerosols (SIA), including nitrate (NO_3^-) and sulfate (SO_4^{2-}), which result from atmospheric chemical reactions involving precursor gases such as NO_x, NH_3, and SO_2. This pathway is widely recognized as a key mechanism contributing to elevated $PM_{2.5}$ levels during winter. Furthermore, significant secondary chemical reactions transpire during nocturnal hours, even in the absence of sunlight. During nocturnal hours, NO_2 reacts with ozone (O_3) to form nitrate radicals (NO_3), which exist in equilibrium with N_2O_5. N_2O_5 has been observed to undergo heterogeneous hydrolysis on aerosol surfaces in the presence of moisture, producing HNO_3. However, in South Korea, observational constraints on the specific nighttime pathways and their quantitative significance remain limited. The ASIA-AQ campaign integrates ground-based observations with atmospheric chemical modeling to ascertain the predominant formation mechanisms of $PM_{2.5}$ during winter.

Q2: Dominant Formation Pathways of Organic Aerosols (What are the primary sources and formation pathways of secondary organic aerosols (SOA) during winter in South Korea?)

Scientific background: Organic aerosols (OA) constitute a significant proportion of the $PM_{2.5}$ mass during the winter months in South Korea. The majority of this OA is not directly emitted; rather, it is formed through atmospheric chemical reactions, leading to the production of secondary organic aerosols (SOA). In light of the ramifications of SOA for air quality and public health, a thorough comprehension of its formation mechanisms is imperative. In general, during summer, biogenic volatile organic compounds (VOCs) emitted from vegetation are the dominant precursors of SOA. However, during the winter months, anthropogenic VOCs

become more prominent due to increased human activity. In metropolitan areas such as the Seoul Metropolitan Area (SMA), VOC emissions originate from a variety of sources, including vehicle exhaust, industrial processes, and solvent use. Among these, aromatic hydrocarbons such as toluene and xylenes are recognized as primary contributors to SOA formation. These compounds undergo complex oxidation reactions in the atmosphere, generating a variety of oxidation products. Environmental factors, such as temperature, oxidant concentrations, and aerosol phase state, influence the specific formation pathways. The objective of this study is to identify the predominant SOA formation pathways and precursor sources under wintertime conditions in South Korea, based on the multi-platform observations collected during the campaign.

Q3: Relative Contributions of Domestic Emissions and Transboundary Influence (What are the relative contributions of local vs. transboundary emissions from different sectors to wintertime $PM_{2.5}$ concentrations in South Korea, including the roles of meteorology and transport pathways?)

Scientific background: It is critical to quantify the relative contributions of domestic and transboundary sources to wintertime $PM_{2.5}$ concentrations in South Korea to facilitate the development of effective air quality management strategies. These contributions are not fixed values; they vary depending on synoptic-scale meteorological patterns across East Asia and the long-range transport pathways of air pollutants. Furthermore, recent initiatives undertaken by East Asian nations to curtail anthropogenic emissions can be expected to alter the balance between domestic and external contributions. Accurate apportionment of source contributions is imperative for the establishment of science-based air quality policies, necessitating a comprehensive modeling approach that integrates outputs from multiple chemical transport models. In this study, a set of seven chemical transport model simulations is employed to quantitatively assess the relative contributions of domestic and transboundary emissions to wintertime $PM_{2.5}$ concentrations over South Korea.

Q4: Evaluation of Model Performance in Simulating $PM_{2.5}$ (How accurately do current atmospheric chemistry models simulate the composition of wintertime $PM_{2.5}$ in South Korea, particularly ammonium nitrate and organic aerosols, and what are the primary sources of uncertainty during high $PM_{2.5}$ episodes?)

Scientific background: Atmospheric chemistry transport models, including CMAQ, WRF-Chem, and GEOS-Chem, are extensively utilized for the prediction of air pollutants, such as $PM_{2.5}$ and surface ozone. The accurate simulation of total $PM_{2.5}$ mass concentrations, as well as their predominant chemical components, enhances not only the reliability of forecasts but also provides a scientific foundation for the development of effective mitigation policies. However, the current atmospheric models employed for air quality forecasting are constrained by several sources of uncertainty, including precursor emission inventories, errors in

meteorological input fields, and the complexity of chemical mechanisms, particularly those involving day- and nighttime reactions and gas-aerosol interactions. These limitations are especially pronounced during periods of elevated $PM_{2.5}$ concentrations, when enhanced model performance is most required. One of the objectives of this campaign is to evaluate the performance of chemical transport models in simulating wintertime $PM_{2.5}$, with a particular emphasis on ammonium nitrate and organic aerosols, and to identify the primary sources of model uncertainty during severe pollution events.

Q5: Validation of Geostationary Environmental Satellite Products (Compared to other remote sensing and ground-based observations, how good are GEMS official products at monitoring regional air pollution and its diurnal variability?)

Scientific background: The Geostationary Environment Monitoring Spectrometer (GEMS), launched by the Ministry of Environment of South Korea, is the world's first geostationary satellite dedicated to atmospheric environmental monitoring. GEMS provides hourly observations over East Asia and offers a unique advantage in capturing the diurnal variation of atmospheric pollutants. Unlike polar-orbiting satellites, GEMS enables frequent and simultaneous observations not only over the Korean Peninsula but also across China, Japan, and Southeast Asia, making it well-suited for tracking the transport of air pollutants and airflow patterns across national borders. During the ASIA-AQ campaign, vertical profiles of trace gases and aerosols were obtained using ground-based instruments (such as PANDORA and AERONET) and aircraft-mounted sensors over the Korean Peninsula, the Philippines, Thailand, and Taiwan. These multi-platform observations provide a valuable opportunity to evaluate the accuracy and applicability of GEMS data products and to assess their reliability and data quality for scientific and policy applications over Asia.

3. Scientific Findings

Q1: Identification of Wintertime $PM_{2.5}$ Formation Mechanisms (What are the dominant chemical mechanisms driving wintertime secondary $PM_{2.5}$ formation in South Korea, and how does nighttime chemistry contribute to this phenomenon?)

Summary of Findings:

During the ASIA-AQ campaign, the observed wintertime $PM_{2.5}$ pollution in South Korea was predominantly attributed to secondary formation, with inorganic species being the dominant contributors. It is noteworthy that during periods of elevated $PM_{2.5}$ concentrations, nitrate contributed approximately 40% of the total $PM_{2.5}$ mass. The majority of the nitrate was found to be associated with the efficient formation of ammonium nitrate under ammonium-rich conditions. The contribution of nighttime heterogeneous reactions was found to be insignificant to the campaign-average total nitrate burden. The most effective strategy for reducing ambient nitrate concentrations is to control emissions of NOx, the primary precursors to nitric acid. However, further research is urgently needed to reduce uncertainties associated with observed ammonia concentrations and the identification of its emission sources.

It is important to understand how PM composition varies depending on PM mass. Figure 1-1 shows the daily average concentrations of aerosol chemical species observed at Korea University during the campaign. NO_3^- demonstrates the most pronounced enhancement with a ratio of approximately 2.9, indicating that its concentration increases nearly threefold when daily average $PM_{2.5}$ levels exceed 25 μg m^{-3} compared to cleaner conditions (< 25 μg m^{-3}). This substantial increase suggests that nitrate formation through secondary processes plays a critical role in driving severe pollution events.

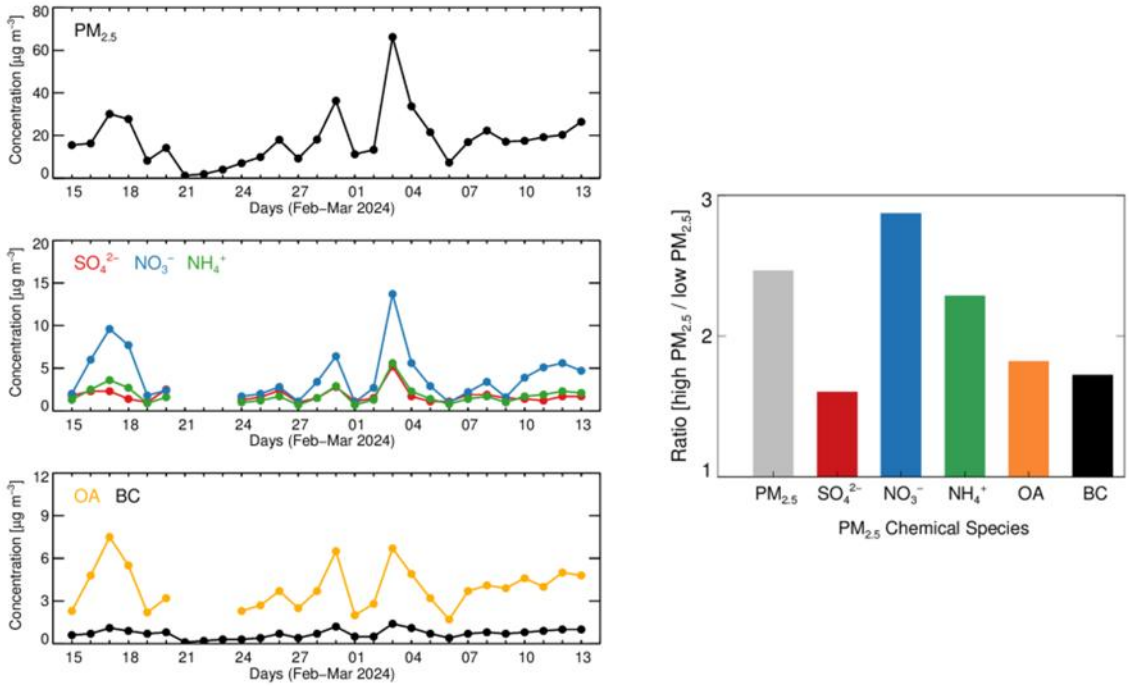

Figure 1-1. (Left) Daily average concentrations of $PM_{2.5}$ chemical components measured at Korea University during the ASIA-AQ campaign. $PM_{2.5}$ mass concentrations were obtained from the urban air quality monitoring site in Dongdaemun, Seoul. (Right) Concentration ratios of $PM_{2.5}$ and its chemical species between high (> 25 μg m^{-3}) and low (≤ 25 μg m^{-3}) daily average $PM_{2.5}$ conditions.

During the ASIA-AQ campaign, airborne observations from both the DC-8 (K-AMS) and King Air 1900D (AMS) showed that the $PM_{1.0}$ aerosols were nearly fully neutralized (Figure 1-2). Measured NH_4^+ concentrations were in close agreement with the stoichiometric amounts required for complete neutralization of sulfate, nitrate and chloride (Predicted NH_4^+), yielding high correlations (R^2 = 0.95-0.99) and slopes approaching unity (0.85-0.87). These results suggest that the availability of ammonium was sufficient throughout the study, indicating that aerosol neutralization was not constrained by a shortage of ammonia. The observation that aerosols were effectively neutralized carries significant implications for the understanding of nitrate accumulation during periods of elevated PM.

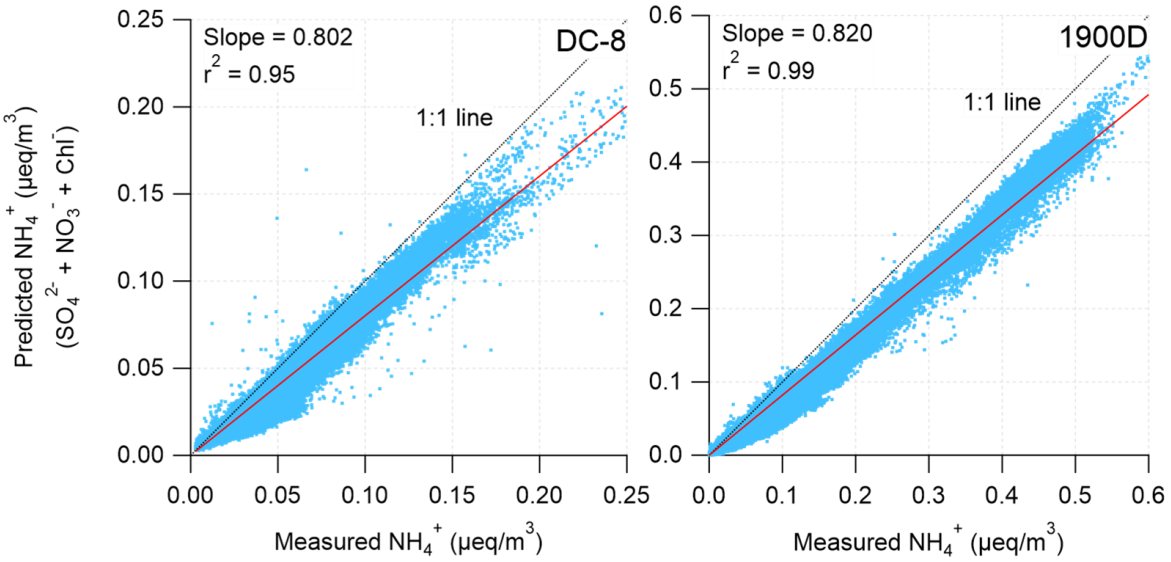

Figure 1-2. Measured versus predicted NH_4^+ concentrations for charge balance with sulfate, nitrate and chloride during the ASIA-AQ campaign from the DC-8 (K-AMS) and King Air 1900D (AMS) research aircraft. Note that AMS measurements represent $PM_{1.0}$ size fraction. Blue dots indicate 1 second measurements, red lines indicate best fits, and gray lines indicate 1:1 lines.

Figure 1-3 presents an indirect assessment of the limiting precursor for daytime inorganic nitrate formation based on aircraft observations. Xu et al. (2019) proposed that when R < 1, ammonia is the limiting precursor, and when R > 1, nitric acid is the limiting precursor. The R values derived from ASIA-AQ observations were generally greater than 1, indicating that inorganic nitrate formation over South Korea generally occurred under nitric acid–limited conditions. Furthermore, the R value exhibited a tendency to be elevated under conditions of low-SNA (sulfate + nitrate + ammonium) and approached a value of 1 as SNA concentrations increased, a finding consistent with the depletion of nitric acid as ammonium nitrate formation progressed.

Taken together, these results suggest that the accumulation of ammonium nitrate in South Korea during winter was facilitated by abundant ammonia, while the availability of nitric acid ultimately constrained further nitrate production. Consequently, achieving effective reductions in daytime inorganic nitrate concentrations necessitates the prioritization of nitric acid level regulation.

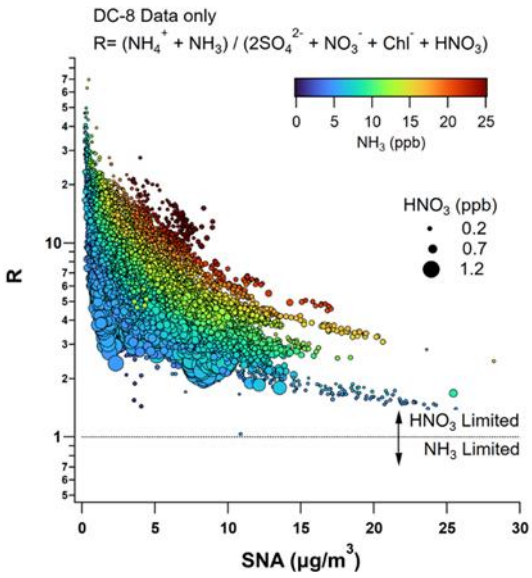

Figure 1-3. Limiting precursor for inorganic nitrate formation during the ASIA-AQ campaign (DC-8 data). R is defined as the ratio of total ammonia to the sum of sulfate (×2), nitrate, chloride, and nitric acid concentrations. R > 1 indicates HNO_3 limitation; R < 1 indicates NH_3 limitation. The x-axis shows SNA (sulfate + nitrate + ammonium), with color representing NH_3 and marker size representing HNO_3 concentrations.

During nocturnal periods, the process of nitrate formation has been observed to occur via N_2O_5, which is produced through the equilibrium between NO_2 and NO_3. Subsequently, N_2O_5 undergoes hydrolysis on particle surfaces, resulting in the formation of HNO_3. In order to evaluate their formation under near-equilibrium conditions, the measured $[N_2O_5]$:$[NO_3]$ ratio was compared with theoretical values calculated from NO_2 concentrations and the thermodynamic equilibrium constant (Keq) (see Figure 1-4). When N_2O_5 concentrations were high, particularly in March (yellow dashed box in Figure 1-4(b)), measured and theoretical ratios were in good agreement. Conversely, when particulate nitrate (pNO_3) concentrations and particle surface areas were elevated, the observed ratios fell below the theoretical predictions (Figure 1-4(a)). This discrepancy suggests active heterogeneous conversion of N_2O_5 to HNO_3 on particle surfaces, contributing to particulate formation (yellow dashed box in Figure 1-4(b)). The maximum concentrations of N_2O_5 and NO_3 were observed between March 13 and 16, a period during which both local emissions and long-range transport processes significantly influenced the air masses over Seoul. During this period, the presence of strong southwesterly winds led to the transportation of O_3-rich air from the Yellow Sea into NO_2-rich urban areas, thereby enhancing N_2O_5 production. The presence of preexisting particles likely promoted heterogeneous conversion, resulting in a decrease in the observed $[N_2O_5]/[NO_3]$ ratio relative to equilibrium. These results underscore the sensitivity of nitrate formation during nocturnal hours to meteorological and chemical conditions (Kim et al., 2026; Lee et al., under review).

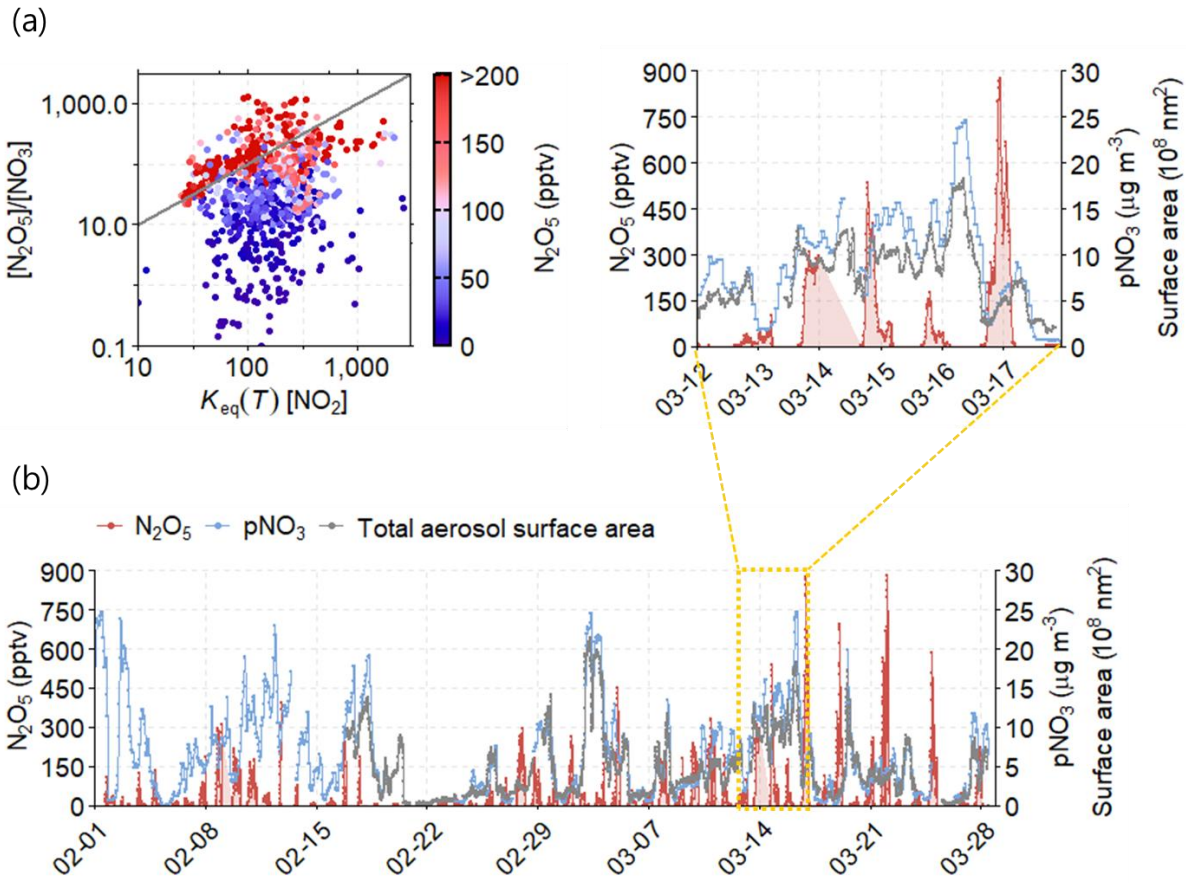

Figure 1-4. (a) Comparisons between the measured N_2O_5 and NO_3 ratios with theoretical values predicted from chemical equilibrium. The x-axis shows theoretical [N_2O_5]/[NO_3] ratios predicted from the equilibrium constant (*K*eq) and measured NO_2 concentrations, while the y-axis shows the observed ratio of [N_2O_5] to [NO_3]. The solid gray line represents the 1:1 relationship between the theoretical and observed ratios. (b) The time-series variations of N_2O_5, particulate nitrate (pNO_3), and total aerosol surface areas measured at Korea University during the ASIA-AQ campaign. The yellow dashed box indicates a period of active heterogeneous conversion of N_2O_5 to HNO_3 on aerosol surfaces.

To better understand nighttime atmospheric chemistry, numerical modeling offers valuable insights into the mechanisms operating under conditions of limited photochemistry. At night, N_2O_5 acts as a temporary reservoir for NO_x and undergoes heterogeneous uptake on aerosol surfaces to form total nitrate (TNO_3, defined as the sum of HNO_3 and particulate NO_3^-). Depending on thermodynamic conditions, TNO_3 can shift into the aerosol phase and contribute to nighttime increases in $PM_{2.5}$ mass. To quantify the impact of N_2O_5 reactions on TNO_3 concentrations, the WRF-GC chemical transport model was used to simulate both absolute and relative contributions of N_2O_5 heterogeneous chemistry. Note that contributions from outside the domain shown in Figure 1-5 were not considered in this analysis.

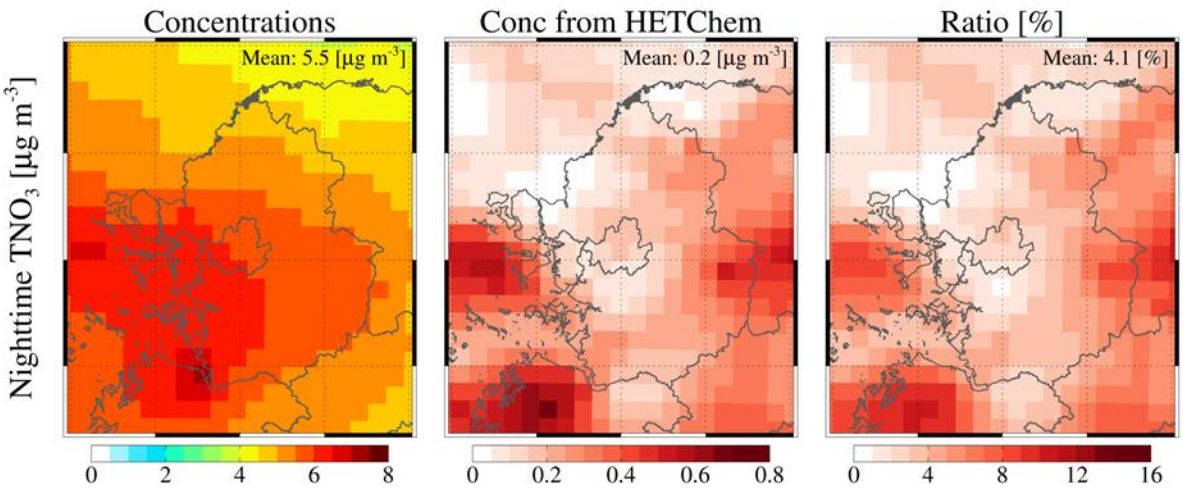

Figure 1-5. Analysis of the impact of nighttime N_2O_5 heterogeneous reactions on total nitrate (TNO_3 = HNO_3 + NO_3^-) concentrations during the ASIA-AQ campaign using the WRF-GC model. (a) Domain-averaged nighttime TNO_3 concentrations modeled over the campaign period; (b) TNO_3 concentrations produced via N_2O_5 heterogeneous uptake; (c) Relative contribution (%) of nighttime N_2O_5 heterogeneous reactions to TNO_3.

Figure 1-5a presents the domain-averaged nighttime TNO_3 concentrations modeled over the campaign period, reflecting both production and transport. Figures 1-5b and 1-5c show the absolute and relative contributions of TNO_3 formed specifically via N_2O_5 uptake within the domain. The results indicate that, on average, N_2O_5 heterogeneous reactions contributed approximately 4% to nighttime TNO_3 concentrations across the domain, with localized maxima of up to 15%. This suggests that, from a campaign-average perspective, nighttime heterogeneous chemistry within the SMA had a relatively minor impact on TNO_3 levels.

Regional variability in N_2O_5 contributions appears to be driven by the balance of NO_x and ozone concentrations. In the SMA, the relative contribution of N_2O_5 reactions was generally low, as high NO_x emissions frequently led to ozone titration, limiting N_2O_5 formation. In contrast, downstream of the SMA, where background ozone and transported NOx were sufficient, provided more favorable conditions for N_2O_5 formation and subsequent heterogeneous nitrate production. Along the western coast of South Korea, where strong aerosol sources such as thermal power plants and petrochemical complexes are located, and where elevated TNO_3 concentrations were modeled, the contribution of N_2O_5 reactions was also enhanced.

Q2: Dominant Formation Pathways of Organic Aerosols (What are the primary sources and formation pathways of secondary organic aerosols (SOA) during winter in South Korea?)

Summary of Findings:

During the ASIA-AQ campaign, organic aerosol (OA) accounted for approximately 20% of $PM_{2.5}$ mass on average. This contribution was found to be comparatively elevated during episodes of low $PM_{2.5}$. The concentration of secondary organic aerosol (SOA) was found to be significantly greater than that of primary organic aerosol (POA). This finding suggests that atmospheric chemical processing plays a significant role in the formation of organic aerosols (OA). Airborne observations indicated that the main contributor to SOA was most likely to be estimated semi-volatile and intermediate-volatility organic compounds (Estimated S/IVOCs), followed by aromatic hydrocarbons. Ground-based measurements identified toluene, among aromatic species, as a significant contributor. These findings indicate the necessity of ongoing management of these emission sources to achieve co-benefits in reducing both wintertime $PM_{2.5}$ and summertime ozone levels.

The sources of OA are highly diverse, and a few have been identified at the VOC species level. The DC-8 and the King Air 1900D were utilized for the purpose of measuring the spatio-temporal variation of OA composition over South Korea during ASIA-AQ. Using the NOx photochemical clock method to analyze DC-8 aircraft observations over the SMA (see Figure 2-1), total OA concentrations increased steadily over 13 hours, with the SOA fraction rising from 56.6% to 78.7%. This finding indicates that SOA formation through photochemical reactions involving VOC precursors directly contributed to OA mass growth during the campaign.

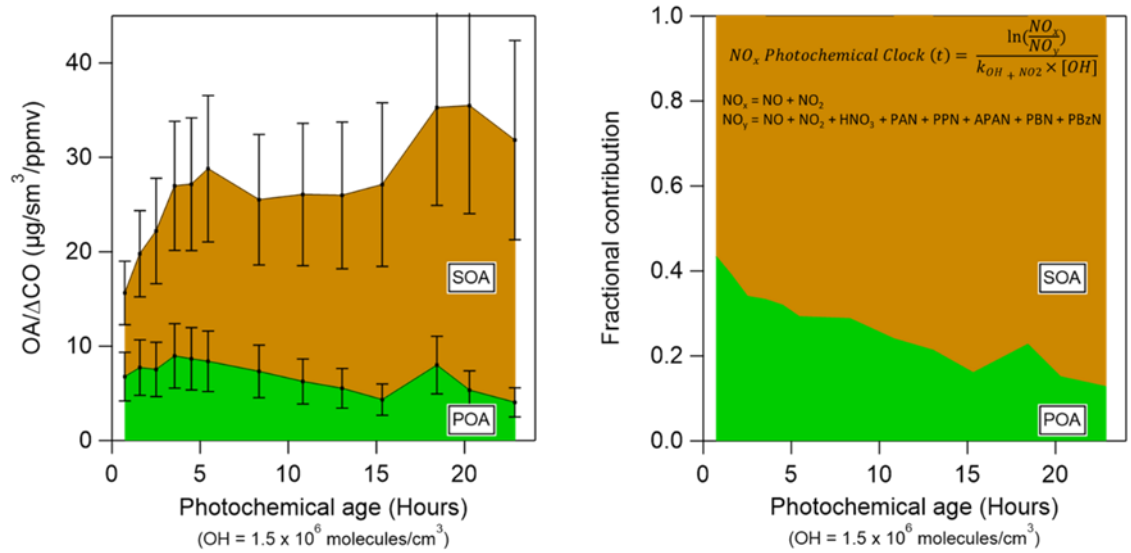

Figure 2-1. Photochemical aging of organic aerosol (OA) during ASIA-AQ, resolved into primary OA (POA) and secondary OA (SOA) using positive matrix factorization (PMF). Data are from five DC-8 flights over the Seoul Metropolitan Area below 2000 m. Error bars indicate OA uncertainty (±38%).

Figure 2-2 shows the contribution of precursor gases to SOA formation (f_{SOA}) over the SMA as a function of photochemical aging, resolved by VOC precursor groups using the method of Nault et al. (2018). Among the precursor groups, the single largest contribution was attributed to estimated semi-volatile and intermediate-volatility organic compounds (S/IVOCs), underscoring the importance of unresolved precursors in SOA formation during wintertime conditions. Among the identified groups, aromatics contributed the most, with the Aromatic 1 group (dominated by toluene and xylenes from traffic and solvent use) exceeding Aromatic 2. Alkanes also contributed, though to a smaller extent, while terpenes were negligible, consistent with low biogenic activity under reduced winter solar radiation.

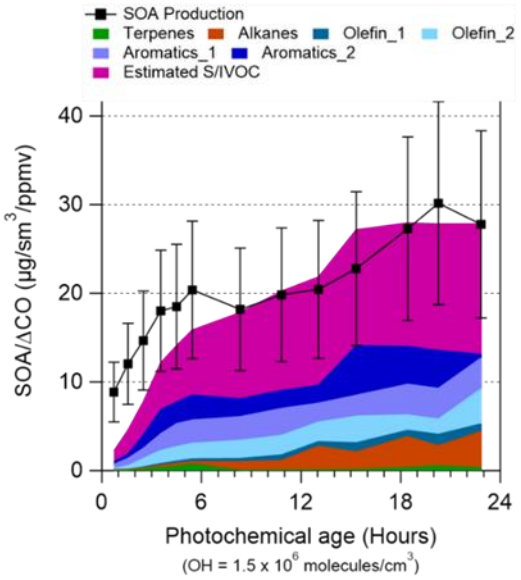

Class	Included compounds
Terpenes	α-pinene, β-pinene
Alkanes (C≤10)	methyl-cyclopentane, cyclohexane, methyl-cyclohexane, n-heptane, *n*-octane, *n*-nonane, *n*-decane
Olefin 1	1-butene, *i*-butene, *cis*-butene, *trans*-butene
Olefin 2	styrene, 1,3-butadiene
Aromatics 1	benzene, toluene, isopropylbenzene, *n*-propylbenzene, ethylbenzene
Aromatics 2	*m*+*p*-xylene, *o*-xylene, 3-ethyltoluene, 4-ethyltoluene, 1,2,3-trimethylbenzene, 1,2,4-trimetylbenzene, 1,3,5-trimetylbenzene
Estimated S/IVOC	6.7[a] x HOA[b]/ΔCO (4.76 μg/sm^3/ppmv)

[a]This value is taken from Dzepina et al. (2009).
[b]Hydrocarbon-like organic aerosol calculated by positive matrix factorization (PMF).

Figure 2-2. SOA production as a function of photochemical age during the ASIA-AQ campaign. SOA concentrations were derived from K-AMS measurements, and VOC-group-based SOA contributions were estimated using WAS measurements following the method of Nault et al. (2018). Data are from five DC-8 flights over the Seoul Metropolitan Area, restricted to altitudes below 2000 m. The error bars represent the uncertainty in OA (±38%).

It is important to acknowledge that the estimated S/IVOC category reflects a pool of precursors that could not be explicitly separated into individual VOC classes. This unresolved category is likely indicative of a mixture of S/IVOCs from multiple anthropogenic sources, including fuel evaporation, incomplete combustion, residential heating and industrial activities. As these precursors were not directly constrained by measurements, their contribution introduces a significant degree of uncertainty into the estimated SOA source apportionment. Consequently, the relative contributions of the identified volatile organic compound (VOC) groups (e.g., aromatics, alkanes) should be interpreted with caution.

The substantial contribution from S/IVOCs underscores a critical limitation in our present capacity to comprehensively characterize the VOCs that drive SOA formation. Given that the concentrations of these S/IVOCs were not directly measured but rather inferred, they are subject to a considerable degree of uncertainty. This ambiguity complicates the interpretation of the relative importance of the VOCs that were explicitly identified, indicating the necessity for both more comprehensive S/IVOC measurements and improved chemical characterization techniques. It is challenging to make a robust comparison of the roles of different VOC classes in SOA production or to design effective control strategies without reducing this uncertainty. Consequently, while the reduction of aromatic VOCs remains a central approach for SOA mitigation in the Seoul Metropolitan Area, the substantial and variable contribution of unresolved S/IVOCs necessitates the pursuit of future research focused on these poorly constrained precursors.

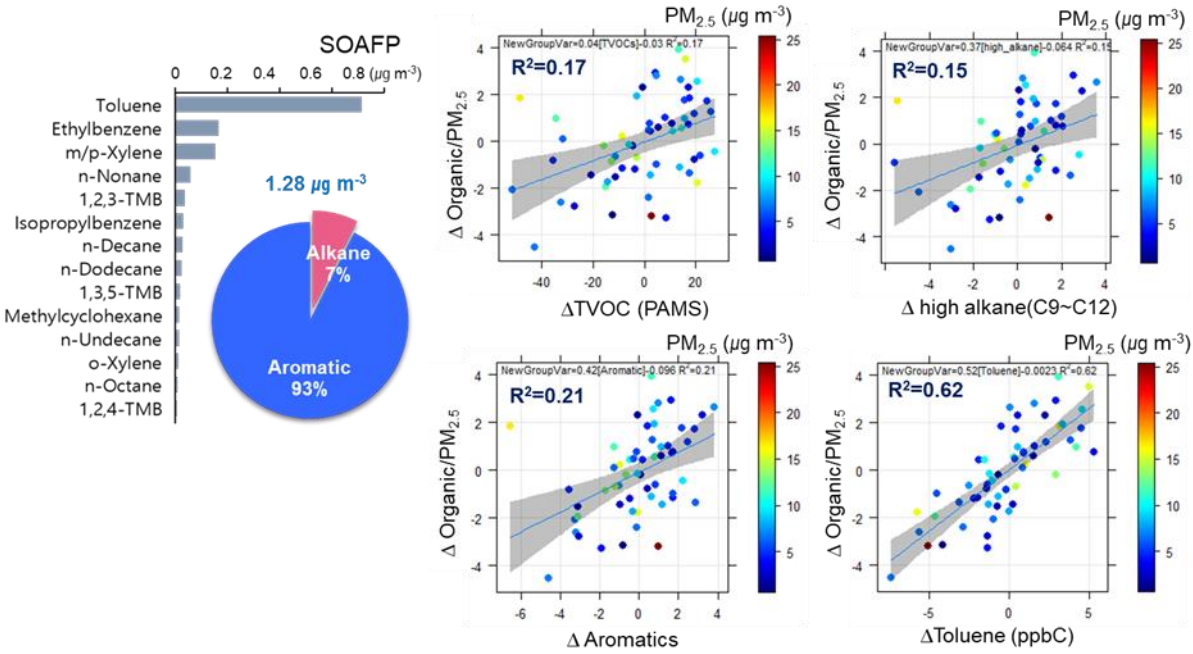

Figure 2-3. Secondary organic aerosol formation potential (SOAFP) by VOC species during the ASIA-AQ campaign (January 25–March 25, 2024), and relationship between daily changes in VOC concentrations (ΔVOC) and changes in the OA-to- $PM_{2.5}$ ratio (ΔOrganic/ $PM_{2.5}$).

The SOA formation potential (SOAFP) of identified VOCs was estimated by multiplying measured individual VOC concentrations by literature-based SOA yields (Grosjean and Seinfeld, 1989). The estimated SOA formation potential (SOAFP) for the specified campaign period (January 25–March 25, 2024) indicated that VOCs had the capacity to produce up to 1.28 μg m^{-3} of OA, accounting for approximately 30% of the measured $PM_{1.0}$ OA (4.3 μg m^{-3}) and around 5% of the total $PM_{2.5}$ mass (Figure 2-3). This finding indicates that in situ OA production from local VOCs during winter months was likely constrained, either due to the exclusion of OVOCs in the SOAFP calculation or due to a significant portion of OA being transported. Among the individual VOCs, toluene exhibited the highest SOAFP.

In order to assess the real-world significance of this theoretical estimate, the daily change in total VOCs (ΔTVOC) was compared with the daily change in the $PM_{1.0}$ organic acid-to-$PM_{2.5}$ ratio (ΔOrganic/$PM_{2.5}$). As groups of VOCs with higher reactivity were considered from total VOCs (TVOC) to high alkanes and aromatics, the correlation with the difference between organic and $PM_{2.5}$ improved. Specifically, increases in high alkanes (C9–C12), which are classified as semi-volatile VOCs, were associated with increases in the OA fraction. Aromatic compounds, especially toluene, exhibited an even stronger relationship, suggesting a substantial contribution to OA formation. The findings of the ASIA-AQ winter campaign suggest that toluene functions as a pivotal indicator in the formation of SOA during winter. Consequently, the implementation of VOC management programs should be a year-round endeavor, not merely a summertime initiative.

Q3: Relative Contributions of Domestic Emissions and Transboundary Influence (What are the relative contributions of local vs. transboundary emissions from different sectors to wintertime $PM_{2.5}$ concentrations in South Korea, including the roles of meteorology and transport pathways?)

Summary of Findings:

During the ASIA-AQ campaign, the relative contributions of external sources and domestic emissions to $PM_{2.5}$ concentrations in South Korea were estimated by averaging the results from seven different chemical transport models, including five that directly participated in the campaign. The dominant contributor was identified as long-range transport of pollutants from China, accounting for approximately ~55% of the $PM_{2.5}$ burden, followed by domestic emissions (~30%) and the rest of the world (~15%). These contributions were found to be highly sensitive to meteorological conditions and subject to uncertainties associated with the meteorological fields used in the models. Satellite-based analyses of long-range transport suggested an even higher contribution (~67%) to $PM_{2.5}$ concentrations. Consequently, the values presented in this study should not be interpreted as absolute, and future assessments will require improved meteorological inputs and updated emission inventories for China.

The present study sought to investigate the contributions from regional emission sources to $PM_{2.5}$ concentrations in South Korea. To this end, the source-receptor relationship of $PM_{2.5}$ was estimated based on results from seven models. Five of these used the Brute-Force Method (BFM), one used the Integrated Source Apportionment Method (ISAM), and one applied the GEOS-Chem adjoint approach. The BFM approach estimates contributions by reducing anthropogenic emissions from a source region by 20% and scaling the resulting change in receptor-region $PM_{2.5}$ concentrations. Although BFM is widely employed, it operates under the assumption of a linear relationship between emissions and $PM_{2.5}$, thus failing to fully capture the complexity of nonlinear chemical interactions. The ISAM approach utilizes the tagging of precursor emissions to trace their transport and chemical transformations, thereby enabling more precise quantification of source-region contributions, including nonlinear chemistry. However, ISAM necessitates more intricate model structures and increased computational resources. The GEOS-Chem adjoint model is a computational tool that calculates the sensitivity of outputs (e.g., $PM_{2.5}$) to input variables (e.g., emissions, initial conditions) in a reverse-time framework. It employs a gradient-based attribution method, which allows for the calculation of the contributions of different inputs to the outputs of interest.

The results are shown in Figure 3-1. Based on the ensemble mean, the largest contributor to South Korean $PM_{2.5}$ concentrations during the campaign was China, with contributions ranging from 36 ± 8% (P2) to 71 ± 9% (P3), and an average of approximately 55 ± 7% over the entire period. This highlights the substantial impact of long-range transboundary pollution from China. Domestic emissions contributed approximately 29 ± 5% on average, ranging from 16 ± 3% (P3) to 43 ± 7% (P2). Contributions from other regions were less than 21±6%, confirming that the primary drivers of $PM_{2.5}$ pollution in South Korea are transboundary transport from China and domestic anthropogenic sources.

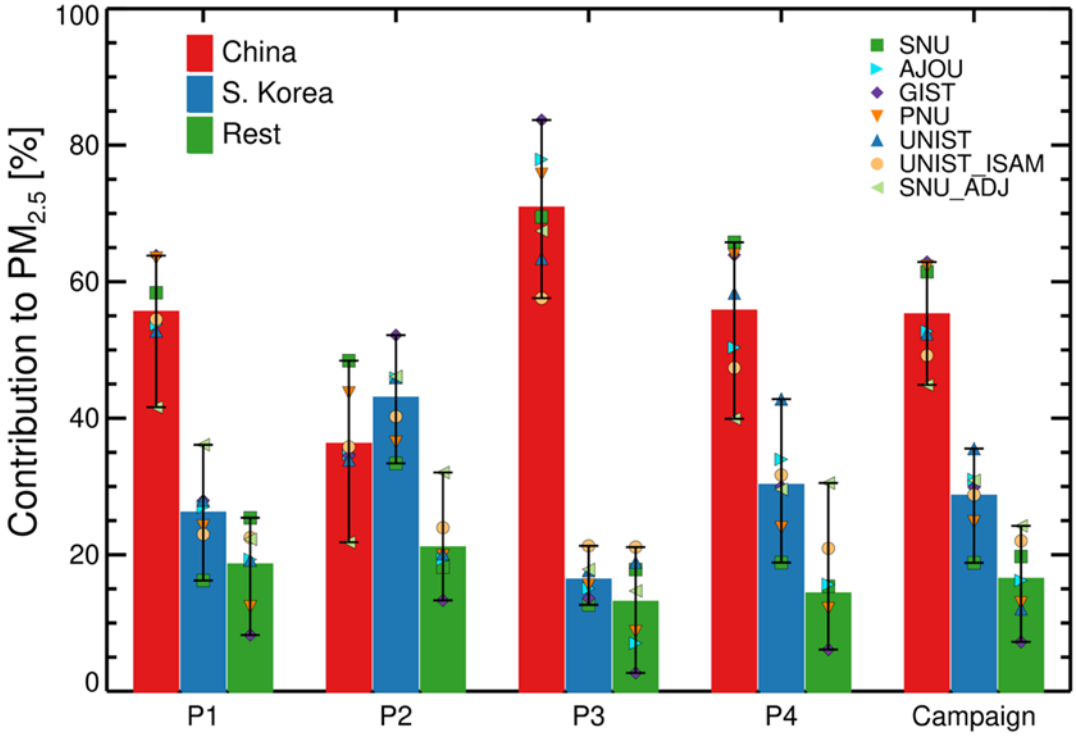

Figure 3-1. Ensemble analysis of $PM_{2.5}$ source contributions from different regions (China: red, South Korea: blue, Other regions: green) during the full campaign and each subperiod: P1 (Relatively High-Concentration Period 1: Feb 1–14), P2 (Clean Period: Feb 15–Mar 2), P3 (Relatively High-Concentration Period 2: Mar 3–8), and P4 (Pollution-to-Clean Transition Period: Mar 9–31). The source contribution analysis was conducted for the entire ASIA-AQ campaign period (February–March 2024). Contributions were estimated using seven models: SNU (WRF-GC), AJOU (CMAQv5.3.2), GIST (CMAQvG), PNU (WRF-Chem), UNIST (CMAQ), UNIST_ISAM (CMAQ_ISAM), and SNU_ADJ (GEOS-Chem_Adjoint). Individual model estimates are indicated by symbols.

However, the distribution of individual model estimates exhibited significant variation by period, suggesting that the uncertainty in source attribution is subject to temporal dynamics. The sources of this uncertainty are multifaceted, including differences in attribution methodology, meteorological inputs, model parameterizations, and chemical mechanism representations. Despite the utilization of a shared emissions inventory, substantial inter-model variability is attributable to discrepancies in chemical speciation and the implementation of processes across models. In order to enhance the reliability of future source apportionment studies, it is important to quantify uncertainties arising from differences in attribution methods and to systematically compare the physical and chemical process representations among models. These efforts will contribute to the development of more accurate and consistent regional source attribution frameworks.

Figure 3-2 provides a detailed breakdown of the Chinese contributions shown in red in Figure 3-1, disaggregated by subregions within China as defined on the map. It shows the extent to which emissions from each subregion contributed to $PM_{2.5}$ concentrations in South Korea during the full ASIA-AQ campaign and each subperiod (P1–P4). The relative contributions from different Chinese regions varied markedly in response to changes in synoptic-scale wind patterns, while the campaign-average distribution exhibited a relatively even spread across regions.

Figure 3-3 presents the average contribution of emissions from China, South Korea, and other regions to five major $PM_{2.5}$ components: SO_4^{2-}, NO_3^-, NH_4^+, BC, and OA. The three secondary inorganic aerosols (SO_4^{2-}, NO_3^-, NH_4^+), which make up the largest fraction of $PM_{2.5}$, showed strong consistency across regions. However, unlike SO_4^{2-}, the contributions of NO_3^- and NH_4^+ were relatively higher from China and South Korea with relatively smaller contributions from other regions. This suggests that NO_3^- and NH_4^+ are more sensitive to the distance from emission sources compared to SO_4^{2-}. This spatial dependence was also reflected in model uncertainty. For SO_4^{2-}, which showed lower domestic contributions, uncertainty was more pronounced for Chinese and other regional contributions due to cumulative uncertainties during long-range transport. In contrast, for NO_3^- and NH_4^+, where domestic contributions were higher, uncertainties associated with South Korea's contribution were also relatively larger.

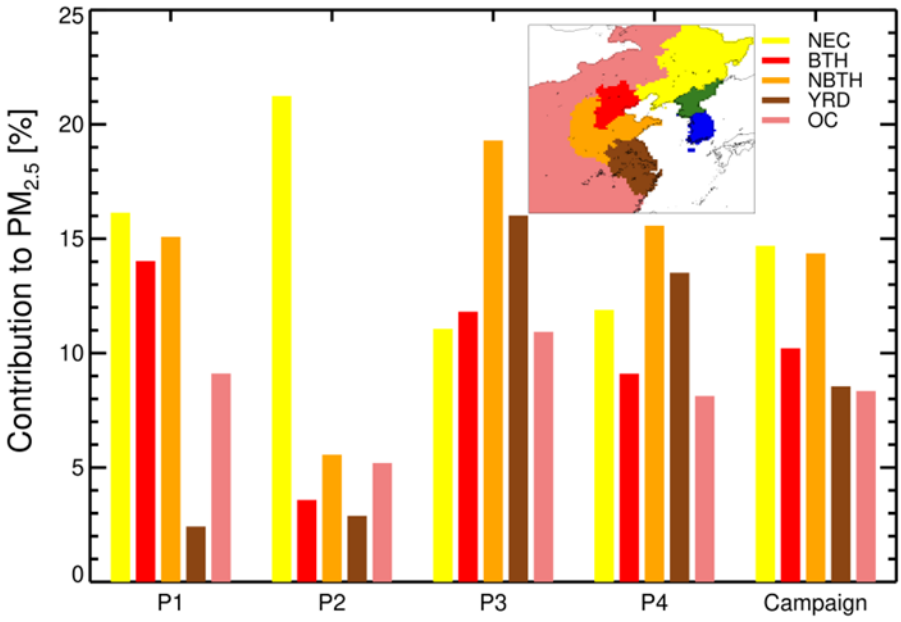

Figure 3-2. Spatially resolved ensemble-mean contributions from individual Chinese subregions to South Korean $PM_{2.5}$ concentrations during the full campaign and each subperiod (P1–P4). Color-coded bars correspond to subregional areas shown on the map. The Chinese subregions are defined as NEC (Northeast China), BTH (Beijing–Tianjin–Hebei), NBTH (Near Beijing–Tianjin–Hebei), YRD (Yangtze River Delta), and OC (Other China).

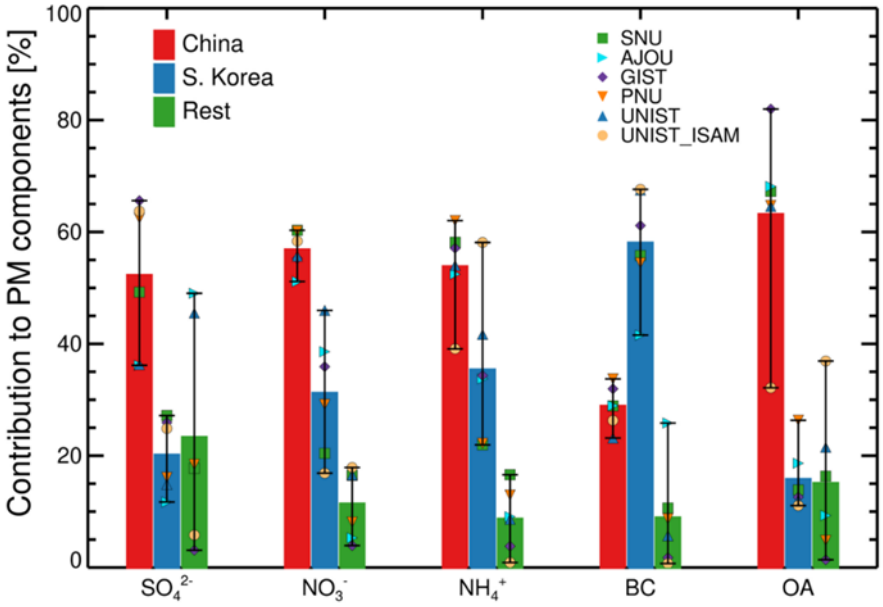

Figure 3-3. Campaign-averaged contributions of regional sources (China: red, South Korea: blue, other regions: green) to $PM_{2.5}$ chemical components (SO_4^{2-}, NO_3^-, NH_4^+, BC, OA). Contributions were estimated using six models: SNU (WRF-GC), AJOU (CMAQv5.3.2), GIST (CMAQvG), PNU (WRF-Chem), UNIST (CMAQ), and UNIST_ISAM (CMAQ_ISAM). Individual model estimates are shown as symbols.

Analysis of refractory black carbon (rBC) properties can provide information to distinguish the influence of local emission from long-range transport. During the ASIA-AQ campaign, the physical characteristics of rBC were measured in central Seoul, including its mass and number concentrations as well as mixing state, which varied significantly depending on air mass origin and the occurrence of high-$PM_{2.5}$ episodes

The relative abundance of these rBC types varied depending on air mass history, $PM_{2.5}$ concentrations, and synoptic meteorological conditions (Figure 3-4). Comparisons of rBC physical properties by period and episode reveal clear differences. rBC measurements included periods characterized by local stagnation (P2-a), long-range transport (P2-b), background continental influence (P2-c), strong inflow (P3), stagnation (P4-a), and upper-level inflow (P4-b). In Figure 3-4, these episodes are color-coded as follows: blue for stagnation, red for transport, gray for background or non-events, and purple for mixed cases.

It is noteworthy that on March 3 (P3), which exhibited the maximum $PM_{2.5}$ concentration, the coating fraction indicated an increase, indicating substantial atmospheric processing and long-range transport (Adachi et al., 2014; Lim et al., 2022; Lim et al., 2023). Conversely, from March 10–17 (P4), $PM_{2.5}$ concentrations remained at relatively low levels, while rBC number

concentration exhibited a notable peak, reaching its highest point during the campaign. Concurrently, rBC CMD (Count Median Diameter) exhibited minimal size, and the coating fraction was low. This finding suggests that local sources, such as vehicular emissions during periods of stagnation, exerted a dominant influence (Lim et al., 2025). The findings indicate that the physical characteristics of rBC, including its number concentration, CMD, and mixing state, function as effective indicators for differentiating between long-range transport and local source influence during the ASIA-AQ campaign.

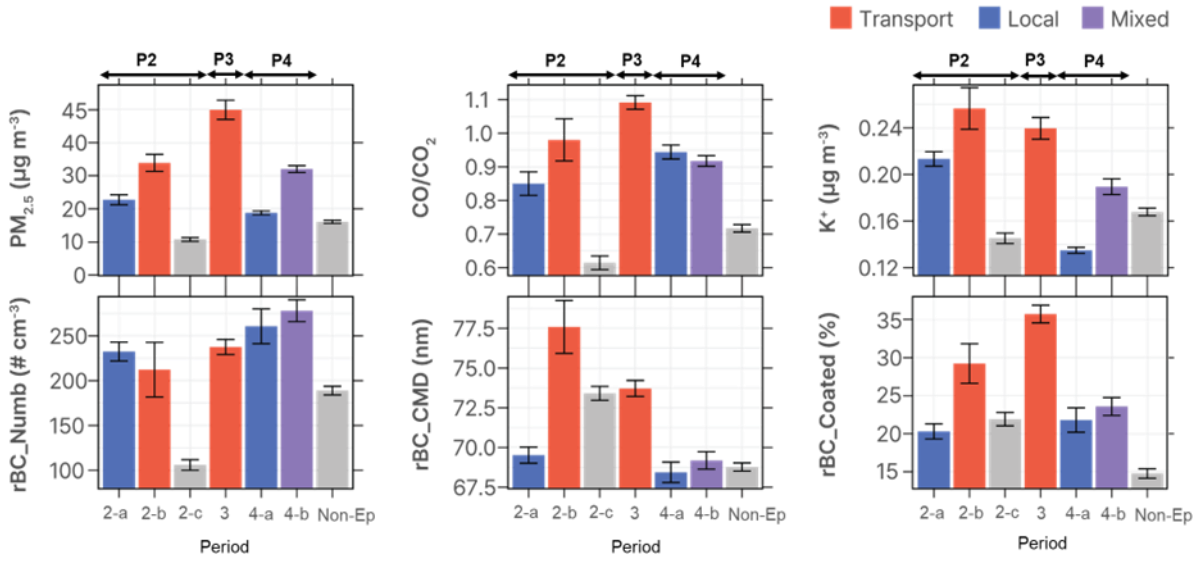

Figure 3-4. Average values of $PM_{2.5}$, CO/CO_2 ratio, potassium (K^+), rBC number concentration (rBC_Numb), count median diameter (rBC_CMD), and coating fraction (Frx_Coated) during the ground observation periods of ASIA-AQ (P2–P4; February 28–March 16, 2024) and selected high-$PM_{2.5}$ episodes. Episodes are defined as P2 (2-a: Feb 28–292-b: Feb 29–Mar 1, 2-c: Mar 1–3), P3 (Mar 3–5), and P4 (4-a: Mar 10–13, 4-b: Mar 13–16). Bar colors indicate air mass types: stagnation (blue), transport (red), background or non-events (gray), and mixed cases (purple).

Satellite-Based Analysis of Long-Range Transport of Air Pollutants

Satellite observations play a critical role in monitoring the long-range, cross-boundary transport of air pollutants. When combined with tools such as backward trajectory analysis, satellite datasets can provide good evidence for assessing transboundary pollution contributions. Please refer to the details of the method in Lee et al. (2021).

Table 3-1. Category-based comparison of PM_{10}, $PM_{2.5}$, and Aerosol Optical Depth (AOD) concentrations observed in Seoul from February to March 2024 (excluding cloudy days), including long-range transport (LRT) event classification.

	Long-Range Transport Days (Mean)	Non-Transport Days (Mean)	Increase Rate (%)
PM_{10} [μg m^{-3}]	56.3	27.5	105
$PM_{2.5}$ [μg m^{-3}]	31.2	18.7	67
AERONET AOD [Unitless]	0.413	0.246	68
GEMS AOD [Unitless]	0.331	0.264	26

A comparison between long-range transport (LRT) and non-LRT periods revealed that $PM_{2.5}$ and AERONET AOD showed mean increases of 66.8% and 68.0%, respectively (Table 3-1). While local emissions contributed to both LRT and non-LRT episodes, the pronounced increase in PM concentrations during LRT episodes suggests the additional loading from transboundary sources. A similar analysis has also been presented in previous studies, which demonstrated that the air quality in South Korea is frequently affected by long-range transport of air pollutants from neighboring countries (Lee et al., 2021; Lee et al., 2019). Because AOD represents the total columnar aerosol optical depth, rather than near-surface particle mass, its relative increase during LRT events tends to be higher than that of surface-level PM concentrations. However, the increase in satellite-based AOD from GEMS was 25.6%, which is lower than the corresponding increase in PM concentrations.

Q4: Evaluation of Model Performance in Simulating $PM_{2.5}$ (How accurately do current atmospheric chemistry models simulate the composition of wintertime $PM_{2.5}$ in South Korea, particularly ammonium nitrate and organic aerosols, and what are the primary sources of uncertainty during high $PM_{2.5}$ episodes?)

Summary of Findings:

Model performance was evaluated by comparing simulation outputs from five models participating in the campaign with both ground-based and airborne observations. The ensemble means, representing the average of the models, were found to reproduce ground-level observations well by reducing uncertainties arising from differing physical and chemical treatments among individual models (e.g., NO_3^- R: 0.46–0.91; NH_4^+ R: 0.40–0.91). The ensemble results showed high correlations with ground observations for NO_3^- and NH_4^+ ($R > 0.89$). However, comparisons with airborne observations revealed a consistent overestimation of inorganic aerosol concentrations in the free troposphere. This overestimation is larger than simply being explained by emission changes and rather likely stems from model process representations.

Model Information Used in the Campaign

Table 4-1. List of regional-scale models participating in the ensemble modeling system and detailed information for each model. All models used the ASIA-AQ v3 emissions inventory.

Model	CMAQv5.3.2	WRF-Chem	CMAQvG	WRF-CMAQ	WRF-GC
Institution	Ajou Univ.	Pusan Nat'l Univ.	GIST	UNIST	Seoul Nat'l Univ.
Meteorology	WRFv4.4	WRFv4.5	WRFv4.1.5	WRFv4.4	WRF-GCv1.0
Boundary conditions	Hemispherical model of CMAQ (U.S. EPA, 2020)	Default vertical profile	Climatological averages from HCMAQ	Default vertical profile	GEOS-Chem global run
Fire emissions	FINNv1.5	FINNv2.5.1 (NRT)	FINNv2.5.1 (NRT)	FINNv2.5.1 (NRT)	QFED2
Biogenic emissions	MEGAN v2.04	MEGAN v2.04	MEGAN v2.1	MEGAN v2.1	MEGAN v2.1
Horizontal resolution (East Asia) [South Korea]	(27 x 27 km^2) [9 x 9 km^2]	(27 x 27 km^2) [9 x 9 km^2]	(15 x 15 km^2) [15 x 15 km^2]	(27 x 27 km^2) [9 x 9 km^2]	(27 x 27 km^2) [9 x 9 km^2]

Table 4-1 summarizes detailed information on the regional-scale models that participated in the ASIA-AQ campaign. These models were used to evaluate and analyze the emissions and behavior of aerosols and trace gases over the Korean Peninsula, as well as to assess model performance. The table includes details such as meteorological input, boundary conditions, natural emissions (excluding anthropogenic emissions), and grid configurations.

All five participating institutions performed simulations using the ASIA-AQ v3 emissions inventory, ensuring that anthropogenic emissions were consistent across models. Therefore, differences in simulated concentrations among models can largely be attributed to variations in meteorological drivers (e.g., meteorological model versions), natural emissions, and the implementation of chemical mechanisms within each model. To minimize the influence of initial conditions and allow models to reach equilibrium, each simulation included a one-month spin-up period.

Emissions Inventory (ASIA-AQ v3.0)

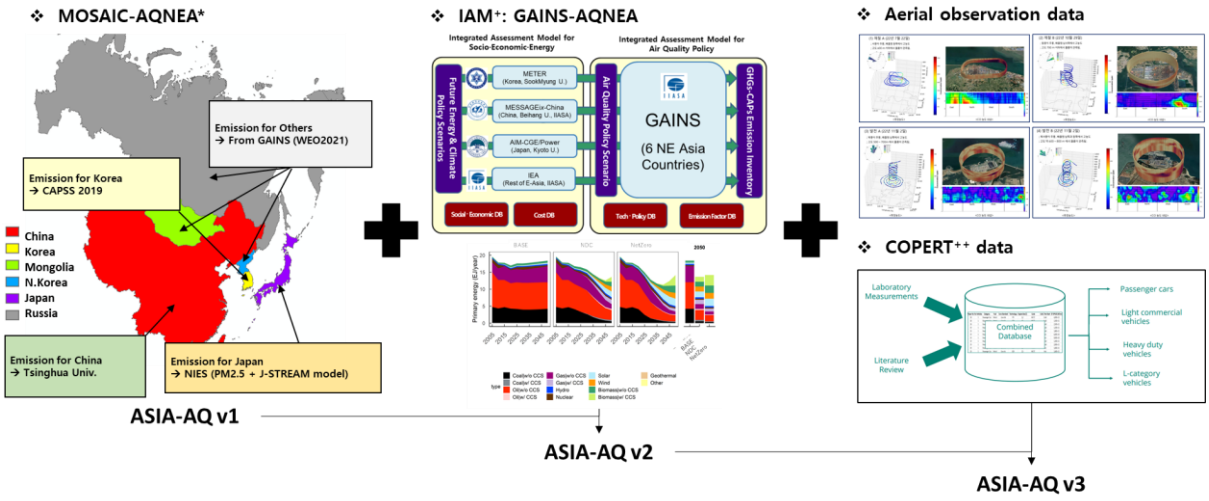

Figure 4-1. Overview of the Update and Integration Process for Developing the ASIA-AQ v3 Emission Inventory. (*AQNEA - Air Quality in NorthEast Asia, $^{+}$IAM - Integrated Assessment Model, $^{++}$COPERT - COmputer Programme to calculate Emissions from Road Transport)

To support the modeling work, an updated regional emissions inventory reflecting the most recent emission status across Northeast Asia was developed by integrating multiple datasets based on the CREATE (Comprehensive Regional Emissions Inventory for Atmospheric Transport Experiment) framework (Figure 4-1). For South Korea, domestic emissions were obtained from the Clean Air Policy Support System (CAPSS) developed by the National Air Emission Inventory and Research Center. For China, Japan, and other Northeast Asian countries excluding Korea, the initial inventory was based on the Mosaic-AQNEA emissions dataset, developed under the Air Quality in Northeast Asia (AQNEA) project.

After the initial inventory (ASIA-AQ v1.0) was prepared, it was provided to the modeling teams for preliminary air quality simulations. Analysis of the simulated concentrations revealed systematic underestimation of several key pollutants, including CO over South Korea and CO, NO_2, and SO_2 over China. To address these discrepancies, efforts were made to incorporate more up-to-date representations of energy-related activity levels. As part of this process, emissions derived from the Greenhouse Gas-Air Pollution Interactions and Synergies (GAINS) model developed by International Institute for Applied Systems Analysis (IIASA) were adopted to update the inventory, resulting in the ASIA-AQ v2.0 emissions dataset. This updated inventory was subsequently delivered to the modeling teams for a second round of simulation experiments.

The results of the second modeling exercise showed substantial improvements in overall model performance across most pollutants and regions. However, CO concentrations

remained persistently underestimated, indicating the need for further refinement of CO emissions. Additional updates were therefore implemented, focusing on both stationary and mobile sources. For stationary sources, emission factors for iron and steel production facilities and coal-fired power plants were revised based on aircraft observation data collected over major industrial complexes and power generation facilities. For mobile sources, emission estimates for South Korea were further evaluated and updated through a review of the European road transport emission model COPERT. The emissions inventory incorporating these additional refinements was designated as ASIA-AQ v3.0 and used as the final emissions dataset supporting subsequent modeling analyses.

Multi-Model Evaluation

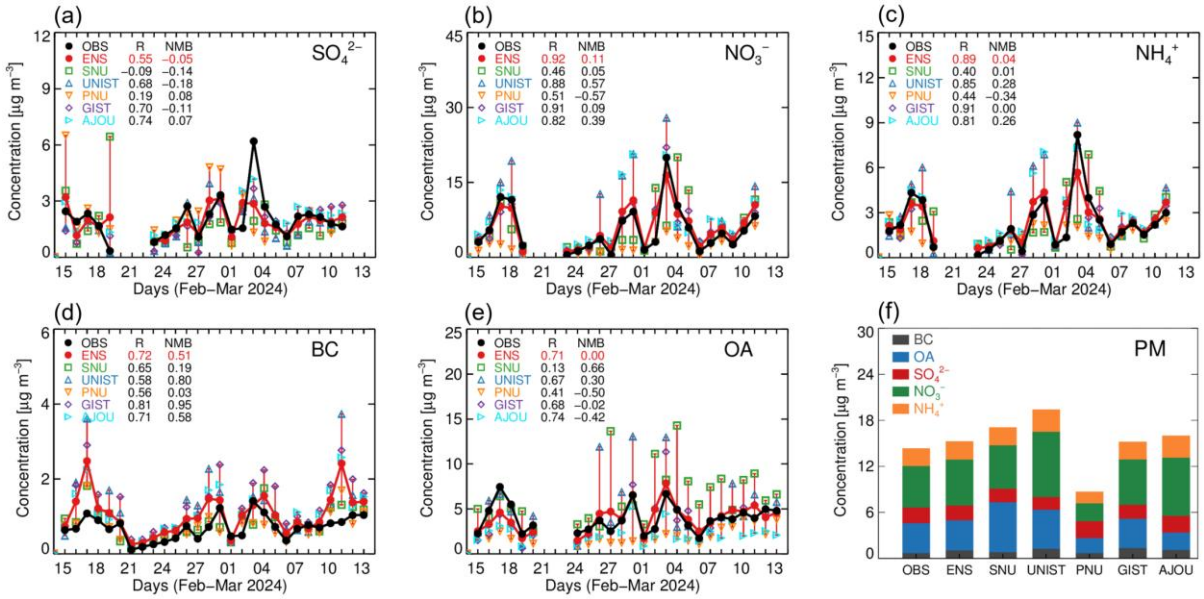

Figure 4-2. Comparison of daily concentrations of (a) SO_4^{2-}, (b) NO_3^-, (c) NH_4^+, (d) black carbon (BC), and (e) organic aerosol (OA) measured at Korea University (OBS) during the ASIA-AQ campaign together with (f) simulations from five regional-scale chemical transport models and their ensemble mean (ENS). Correlation coefficients (R) and normalized mean bias (NMB) with respect to observations are provided for each model and the ensemble.

Figure 4-2 compares major PM components measured at Korea University during the ASIA-AQ campaign with outputs from five regional-scale atmospheric chemistry models used in the study. Each model employs different physical and chemical schemes, resulting in model-to-model differences. Despite these differences, the multi-model ensemble (ENS) reproduced the observed concentrations the most consistently, indicating that the ensemble approach effectively compensates for individual model biases.

Specifically, for secondary inorganic aerosols (SO_4^{2-}, NO_3^-, NH_4^+) and organic aerosol (OA), the ensemble showed low NMB values ranging from –5% to +11% and successfully captured the temporal variability of concentrations. This suggests that the ensemble effectively replicates the day-to-day trends observed during the campaign. In particular, the correlation coefficients between the ensemble and observations for NO_3^- and NH_4^+ exceeded 0.89, demonstrating excellent skill in reproducing the variability of these species.

These findings underscore the utility of ensemble modeling in reducing simulation uncertainties and inter-model divergence. By offsetting the limitations of individual models, the ensemble enhances the overall credibility of simulation results and enables more accurate prediction and interpretation of PM composition for scientific and policy purposes.

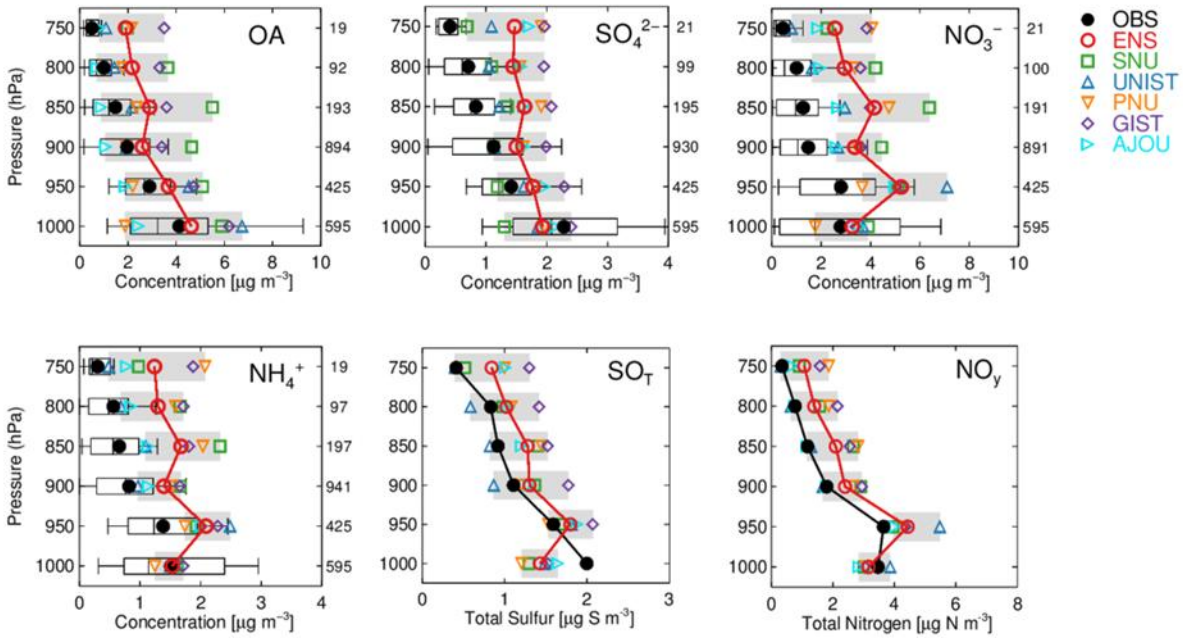

Figure 4-3. Comparison of aerosol vertical profiles from DC-8 aircraft observations and model simulations during the ASIA-AQ campaign. Observations are shown by box-and-whisker plots (interquartile ranges and 10th–90th percentiles) with black circles indicating observed means. Red circles indicate the ensemble mean (ENS), and other colored symbols indicate individual models. Vertical profiles of total sulfur (SO_T, defined as SO_2 + sulfate) and reactive nitrogen (NO_y, including NO + NO_2 + HNO_3 + PAN + particulate nitrate) are also shown. The number of data points used to calculate mean values at each level is shown on the right y-axis.

Figure 4-3 compares vertical profiles of organic and secondary inorganic aerosols measured by the DC-8 aircraft with simulations from the five regional-scale models and their ensemble. Near the surface, the ensemble simulations generally reproduced the observed ranges of aerosol concentrations well. However, in the free troposphere, the ensemble tended to significantly overestimate aerosol levels. This overestimation of secondary inorganic aerosols aloft likely reflects either an overestimation of upwind precursor emissions in the emissions inventory (e.g., SO_x, NO_x) or overly aggressive assumptions in the conversion of gas-phase precursors to particles, particularly via heterogeneous or aqueous-phase reactions.

To further examine this behavior, vertical profiles of total sulfur and total nitrogen were also analyzed. Both species showed good agreement between ensemble and observations near the surface, but pronounced overestimations in the free troposphere. However, model simulations in the Beijing–Tianjin–Hebei (BTH) region, which significantly influences wintertime pollution transport to South Korea, showed reasonable agreement with observations

for $PM_{2.5}$ concentrations (not shown). This suggests that the free-tropospheric overestimation is not primarily due to upwind emission issues but rather to model process representations.

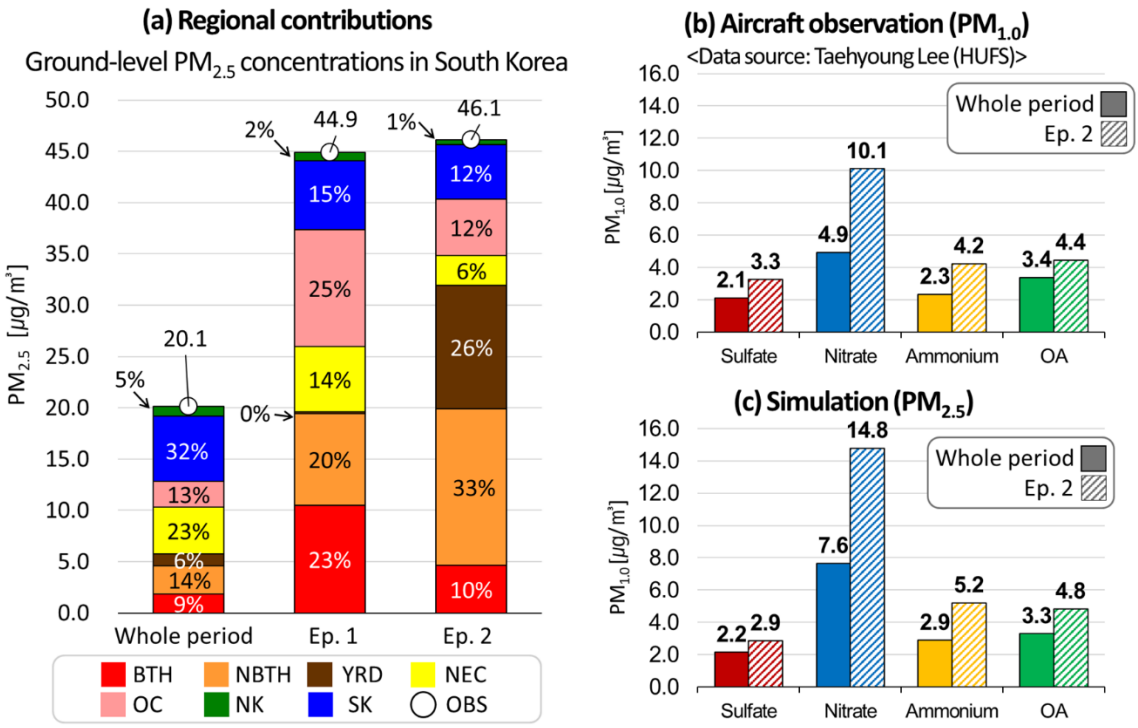

Figure 4-4. (a) Comparison of source-regional contributions to $PM_{2.5}$ concentrations in South Korea during the 2024 ASIA-AQ campaign, including two high-pollution episodes (Ep. 1: 11–12 February 2024; Ep. 2: 3–4 March 2024); (b) Changes in key chemical composition during normal vs. a selected high-pollution episode, based on observed $PM_{1.0}$ from aircraft measurements; (c) Simulated $PM_{2.5}$ chemical compositions at the corresponding aircraft sampling locations for the same episode. Source regions include BTH (Beijing–Tianjin–Hebei), NBTH (Near-BTH), YRD (Yangtze River Delta), NEC (Northeast China), OC (Other China), NK (North Korea), SK (South Korea), and OBS (Observation). The regional domain classification is given in Figure 3-2.

Figure 4-4 shows that during two high-$PM_{2.5}$ episodes, defined as two consecutive days with daily average $PM_{2.5}$ exceeding 35 μg m^{-3} (Ep. 1: February 11–12; Ep. 2: March 3–4), the contribution to ground-level $PM_{2.5}$ from Chinese sources was approximately three times higher than the campaign mean.

In Ep. 1, a sharp increase in $PM_{2.5}$ concentrations was observed in China, likely due to temporary emissions associated with Lunar New Year celebrations. However, these episodic enhancements were not reflected in the model simulations (see Figure 4-5). During Ep. 2, $PM_{2.5}$ concentrations over South Korea increased relative to pre- and post-episode background levels,

whereas no comparable enhancement was observed over China. The model reproduced this event and also captured a significant enhancement of nitrate during this period.

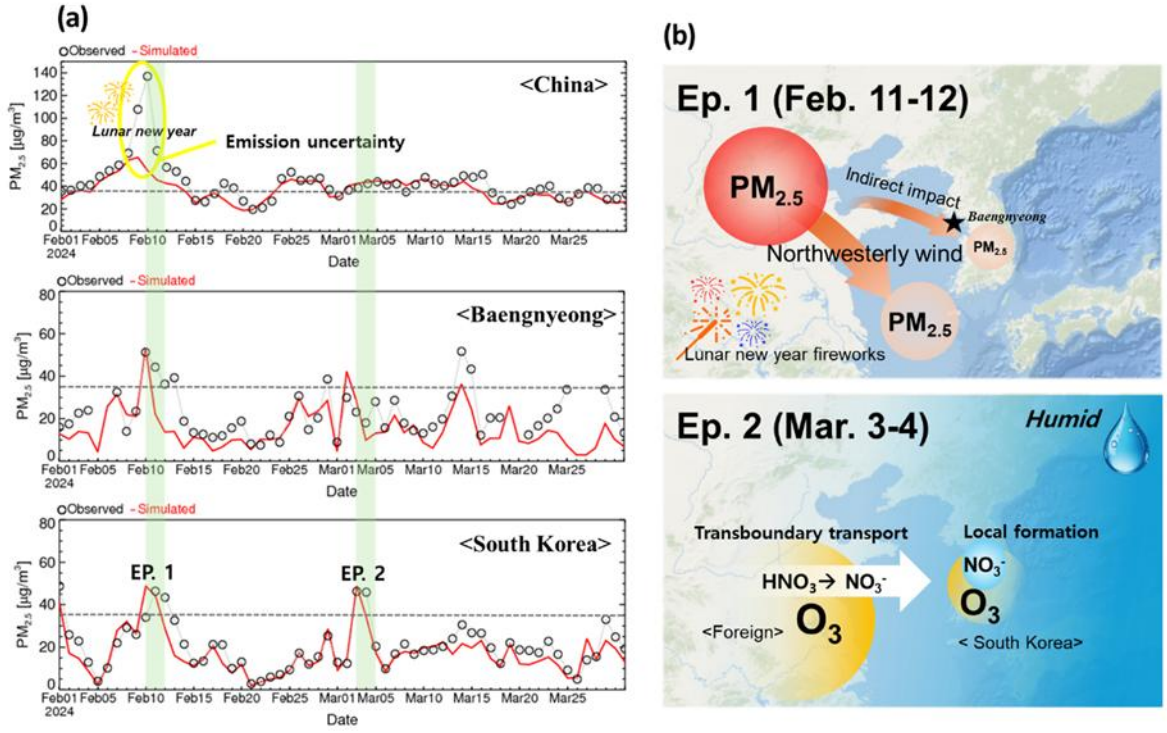

Figure 4-5. (a) Left panels show comparisons between observed and simulated $PM_{2.5}$ concentrations during the 2024 ASIA-AQ campaign; (b) Right panels show conceptual diagrams outlining key factors contributing to uncertainty in $PM_{2.5}$ model simulations during Ep. 1 (Feb 11–12) and Ep. 2 (Mar 3–4).

During Ep. 1, $PM_{2.5}$ concentrations in Baengnyeong were underestimated by the model. This underestimation is likely due to the omission of short-term emission increases, such as fireworks associated with the Lunar New Year, in the bottom-up emissions inventory (Figure 4-5a). In contrast, during Ep. 1, the ensemble and several individual models reproduced nitrate at magnitudes comparable to observations, whereas sulfate was underestimated by most models (Figure 4-2). Because inorganic ions (nitrate, sulfate, ammonium) were anomalously elevated on those days, faithful simulation of their formation and partitioning is critical for source attribution and identification of dominant precursors under high-$PM_{2.5}$ conditions. For OA, the ensemble captured the observed variability, but individual models diverged (with some overprediction and others showing underprediction), highlighting the need to improve organic aerosol representation. Priorities are to improve sulfate formation (aqueous/heterogeneous), NH_3–NO_3^-–SO_4^{2-} thermodynamics with realistic relative humidity (RH), and OA formation/partitioning, with all changes evaluated against observations.

Validations of NH_3 Emissions Using Aircraft Observations

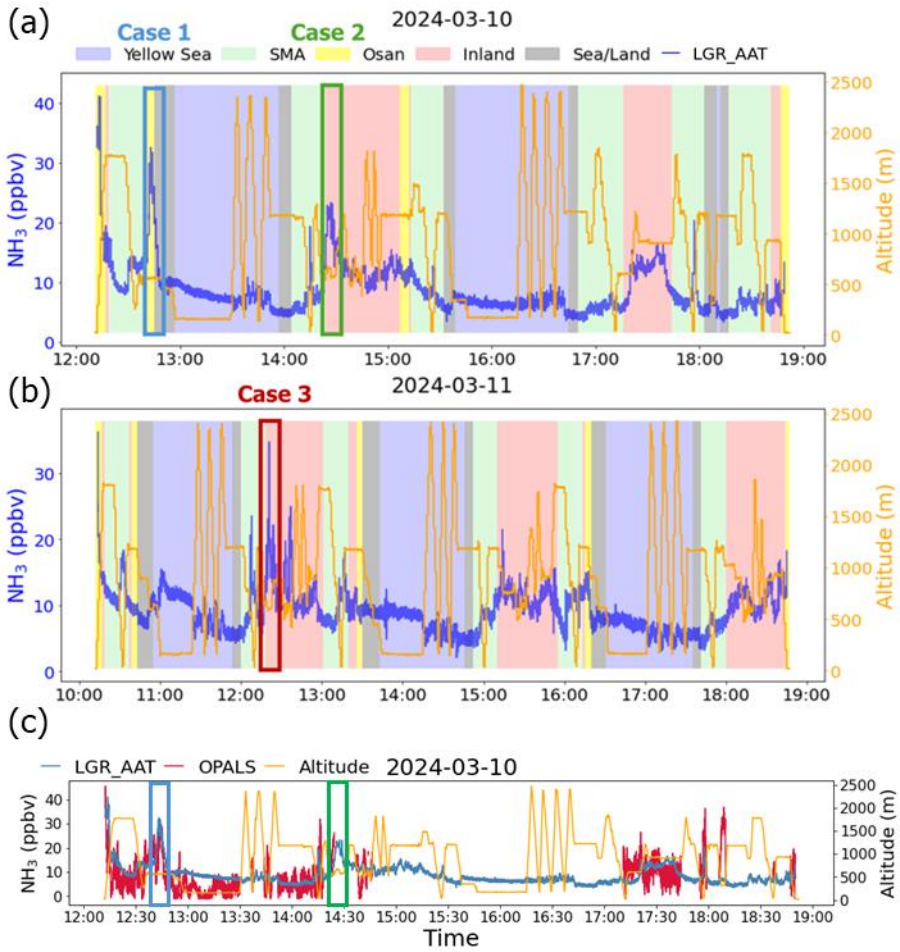

Figure 4-6. NH_3 mixing ratios measured by LGR-AAT (blue) and DC-8 altitude profiles (orange) with (a) blue and green boxes indicating Case 1 and Case 2 on March 10, and (b) the red box highlighting Case 3 on March 11; (c) Time series of NH_3 mixing ratios measured by LGR-AAT (blue) and OPALS (red) on March 10, with the blue and green boxes indicating Case 1 and Case 2, respectively.

During the DC-8 flights, we observed persistently elevated levels of NH_3 over inland Korea, especially in southern Gyeonggi Province (e.g., Osan and Anseong). Three distinct cases were identified, each with a maximum altitude between 500 and 700 m (see Figure 4-6a). Case 1 occurred over Osan Air Base, and Cases 2 and 3 occurred over Daedeok-myeon in Anseong. The mean NH_3 mixing ratios in these cases exceeded the campaign average by a wide margin. To verify data reliability, we compared our results with OPALS, the second onboard NH_3 instrument (see Figure 4-6b). There was generally good agreement between the two instruments for Cases 1 and 2 on March 10, with both instruments capturing the peaks. However, OPALS data were unavailable for Case 3.

Because the hotspot areas are predominantly rural, we hypothesized that livestock is the dominant NH_3 source. To test this, we analyzed two independent datasets: (i) the CAPSS 2021 NH_3 inventory and (ii) livestock-based emissions derived from animal distributions and emission factors (EFs) (Faulkner and Shaw, 2008). For comparability, CAPSS emissions were aggregated to a 3 × 3 km grid, and livestock emissions were computed using the 2020 livestock census with ranges of published EF values (Table 4-2). Emissions from both approaches were then mapped over the hotspot region (Figure 4-7).

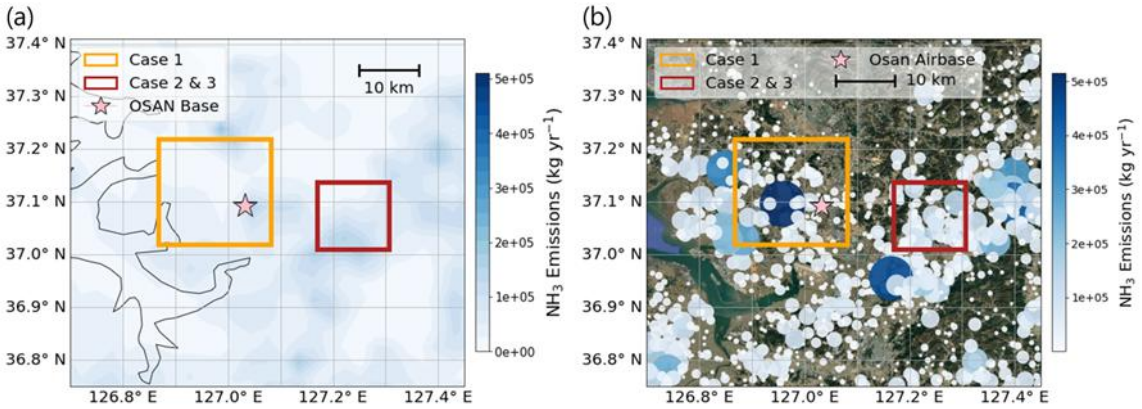

Figure 4-7. NH_3 emissions over the hotspot region derived from (a) CAPSS 2021 and (b) livestock population data combined with emission factors (EFs).

As shown in Figure 4-7, Case 1 exhibits clear differences in both spatial pattern and NH_3 emission intensity between livestock-based estimates and CAPSS 2021; comparable totals arise only under lower-bound livestock EFs. In Cases 2-3, spatial patterns are very similar, but CAPSS shows region-dependent increases exceeding twofold compared to Case 1, whereas livestock-based estimates change little (Table 4-2). EDGAR 2022 provides the lowest bottom-up values, approximately 2-5 times lower than CAPSS 2021 (Table 4-2). As an independent benchmark, we derived top-down NH_3 emissions from aircraft measurements using two dispersion approaches (box and Gaussian plume) on the same grid. These estimates are up to seven times higher than CAPSS 2021 (and even higher relative to EDGAR 2022) but align with the maximum livestock-based EF cases. These results indicate that CAPSS substantially underestimates NH_3 emissions in hotspot regions, particularly in intensive-livestock areas. The results underscore the need for careful EF selection in inventory development and evaluation, given the large spread among EF values.

Table 4-2. Estimated NH_3 emissions in hotspot regions based on aircraft observations over the selected areas (Unit: mmol km^{-2} s^{-1}).

Emission model	Case 1	Case 2	Case 3
Bottom-up			
CAPSS 2021	9.8	22.6	22.6
EDGAR 2022	4.5	4.7	4.7
Livestock based	8.5–75.6	5.1–71.4	5.1–71.4
Top-down (airborne)			
Box approach	72.7 ± 38.1	70.0 ± 36.5	87.7 ± 45.1
Gaussian approach	77.8 ± 39.2	53.9 ± 27.2	68.2 ± 34.9

Q5: Validation of Geostationary Environmental Satellite Products (Compared to other remote sensing and ground-based observations, how good are GEMS official products at monitoring regional air pollution and its diurnal variability?)

Summary of Findings:

Launched in February 2020, the Geostationary Environment Monitoring Spectrometer (GEMS), the world's first geostationary satellite dedicated to atmospheric composition, has successfully monitored multiple air quality indicators across the Korean Peninsula and the broader Asian continent, including AOD, NO_2, SO_2, O_3, HCHO, and CHOCHO. Using in-situ, airborne, and ground-based remote sensing datasets collected during the ASIA-AQ campaign, the performance of GEMS retrievals was evaluated. Building on the Korea-focused analysis in the preceding section, we now extend the evaluation to East and Southeast Asia (the Philippines, Taiwan, and Thailand). Because GEMS provides geostationary, time-resolved coverage across Asia, assessing performance at a broad regional scale aligns with the campaign's objectives. Expanding beyond Korea both overcomes limitations in spatial representativeness and environmental diversity and fully leverages accumulated high-quality ground- and airborne observations, thereby strengthening the statistical robustness and representativeness of the satellite validation. Validation results showed accuracy levels comparable to those of polar-orbiting satellites, with correlation coefficients of R = 0.66–0.74 for AOD, R = 0.83–0.88 for NO_2, R = 0.70 for SO_2, R = 0.99 for O_3, R = 0.53 for HCHO, and R = 0.57 for CHOCHO. Importantly, GEMS demonstrated the ability to resolve the diurnal variability of atmospheric pollutants, an observation capability not available from polar-orbiting satellites. This temporal resolution is expected to provide a critical scientific foundation for the development of future air quality policies. Nevertheless, residual errors and limitations in GEMS retrievals remain. Continued improvement of a priori inputs, particularly those derived from routine aircraft observations and modeling, will be essential for enhancing the accuracy and scientific utility of GEMS data products in the future.

In February 2020, the Ministry of Environment of Korea and the National Institute of Environmental Research (NIER) launched the world's first geostationary environmental satellite, the Geostationary Environment Monitoring Spectrometer (GEMS), which has since been successfully monitoring air quality across the Korean Peninsula and much of Asia (Figure 5-1).

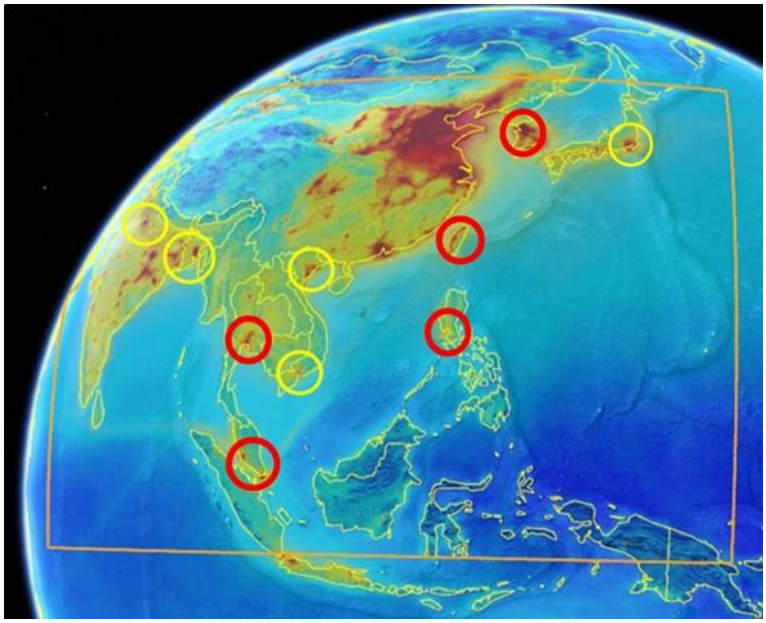

Figure 5-1. Observing domain for GEMS (orange box) and candidate locations for airborne sampling during ASIA-AQ. Yellow circles indicate the original areas of interest and engagement, while red circles indicate the locations that were considered for flight sampling, with four of the five ultimately sampled (i.e., Philippines, South Korea, Taiwan, and Thailand). The overlaid colormap shows annual average nitrogen dioxide (NO_2) concentrations observed by the TROPOMI satellite with red colors indicating the most polluted locations. Candidate locations included: Seoul, South Korea; Tokyo, Japan; Taiwan; Manila, the Philippines; Hanoi and Ho Chi Minh City, Vietnam; Bangkok, Thailand; Kuala Lumpur, Malaysia; Singapore; Dhaka, Bangladesh; and Kolkata and Delhi, India. (Source: ASIA-AQ white paper)

GEMS delivers near real-time hourly observations (up to 6–10 times per day) of a wide range of atmospheric pollutants across Asia during daylight hours, including AOD and trace gases such as NO_2, O_3, SO_2, formaldehyde (HCHO), and glyoxal (CHOCHO). However, the accuracy of the concentrations of these products is influenced by numerous factors, including surface reflectance, solar zenith angle, assumptions on vertical profiles used in retrieval algorithms, meteorological conditions, and topographic complexity. Therefore, continued validation and algorithm refinement are essential to ensure the quality and reliability of GEMS data.

The ASIA-AQ campaign collected extensive in-situ, airborne, and ground-based remote sensing data, providing a robust foundation for satellite retrieval validation. Aircraft

observations offer high-spatial-resolution measurements of various atmospheric species. In particular, the GeoCAPE Airborne Simulator (GCAS) onboard the Gulfstream-III (G-III) aircraft captured horizontal distributions of total column NO_2, while the High Spectral Resolution Lidar (HSRL) provided vertical profiles of aerosols and ozone. These measurements enabled more accurate evaluation of satellite products and played a key role in validating GEMS outputs. During the campaign, two research aircraft, NASA's DC-8 and G-III, were involved in satellite validation activities, generating a rich airborne dataset.

Ground-based remote sensing observations, which measure the atmospheric column from the surface upward, are less affected by surface reflectance and typically provide more accurate vertical column density (VCD) values than satellite retrievals. For this reason, they are commonly used as ground-truth references for satellite and aircraft data validation. In the ASIA-AQ campaign, additional ground-based instruments such as Pandora spectrometers and AERONET (AErosol RObotic NETwork) sun photometers were deployed across Gyeonggi and Chungcheong Provinces within the G-III flight domain. This deployment aimed to improve spatial representativeness at the GEMS pixel scale and reduce uncertainties related to sub-pixel variability.

Through this intensive observation campaign, the ASIA-AQ effort is expected to contribute not only to the improved validation and refinement of GEMS data products, but also to the advancement of atmospheric monitoring systems in the region. Aircraft observations serve as a critical link between satellite and surface measurements, and continued algorithm improvements based on these observations will be essential to enhancing GEMS performance. Looking forward, the availability of high-quality, validated GEMS data is anticipated to strengthen the scientific basis for atmospheric pollution monitoring and climate research. In turn, this will support more effective, evidence-based environmental policymaking in Asia.

Validation of GEMS Geostationary Satellite Products

◎ Aerosol Optical Depth (AOD, Version 2.1)

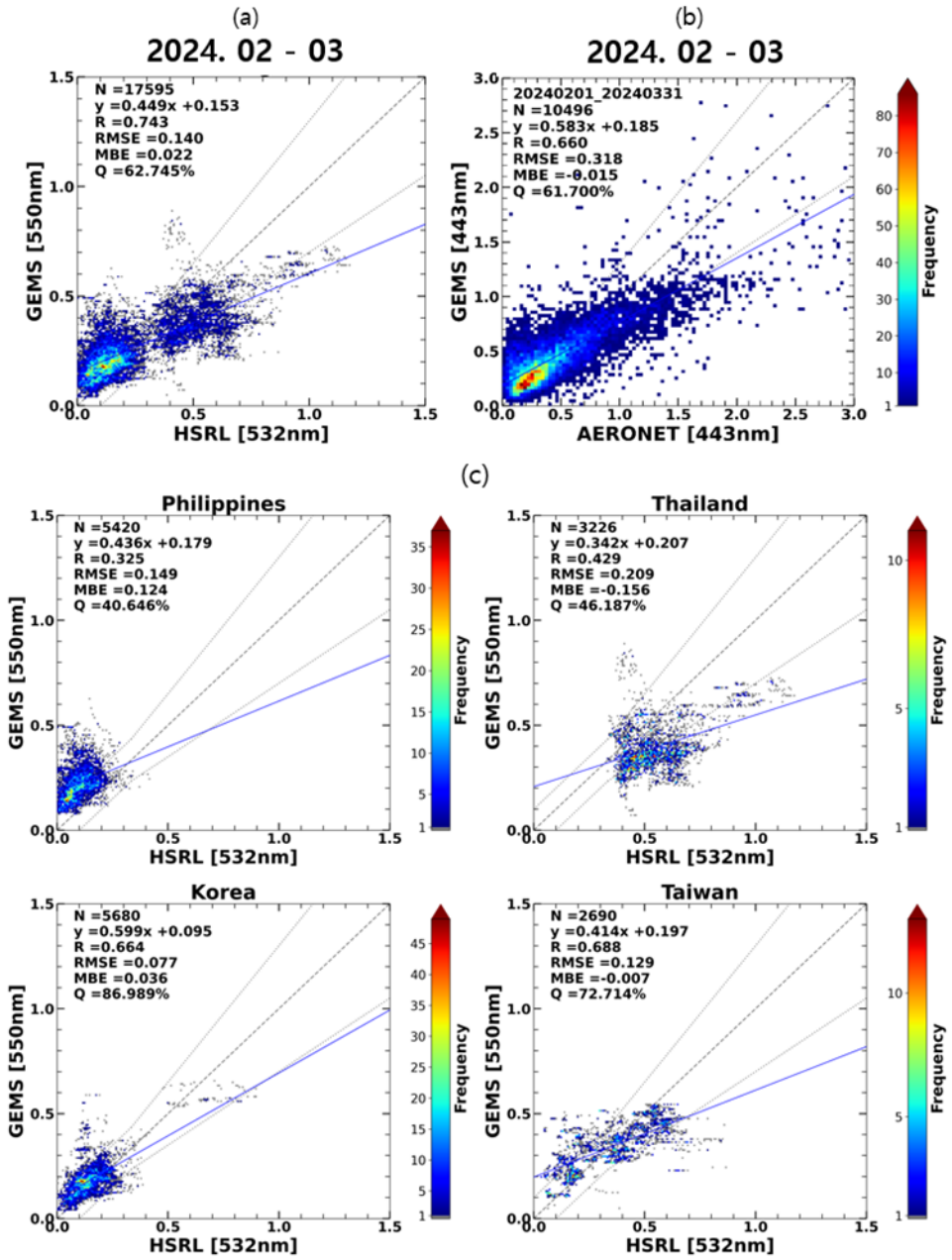

Figure 5-2. (a) Scatterplot comparing GEMS AOD [550 nm] with HSRL AOD [532 nm]. Temporal matching was conducted by averaging HSRL observations within ±30 minutes of the GEMS overpass time, and spatial matching was based on averaging GEMS AOD values within a 25 km radius of the HSRL observation pixel. (b) Scatterplot comparing GEMS AOD [443 nm] with AERONET AOD [443 nm] using the same temporal and spatial collocation criteria as in (a). (c) Country-level comparison of GEMS AOD [550 nm] and HSRL AOD [532 nm] using the same matching criteria. The dashed line with wider spacing indicates the 1:1 line (y = x), and the narrower dashed lines represent the larger of ±0.1 or ±30% error bounds. RMSE

(Root Mean Square Error) and MBE (Mean Bias Error) are displayed within the figure. The Q value represents the fraction of data points falling within this error range.

During the ASIA-AQ campaign, validation of GEMS aerosol products against the vertical profiling instrument HSRL onboard the G-III aircraft was conducted using consistent criteria for AOD (Figure 5-2). Relatively stable validation results were obtained in South Korea and Taiwan, with correlation coefficients (R) of 0.66 and 0.69, and Q values of 87% and 73%, respectively, indicating high reliability. In contrast, validation performance declined in the Philippines due to cloud contamination, and in Thailand, AOD was consistently underestimated due to high surface reflectance over parts of the Indochina Peninsula. Overestimation of surface reflectance at 550 nm appeared to further amplify this underestimation.

Among the GEMS aerosol optical depth (AOD) retrieval products (Cho et al., 2024), the AOD at 550 nm was selected for intercomparison with HSRL observations. GEMS AOD at 550 nm tended to be underestimated relative to HSRL (airborne) and AERONET (ground-based) observations. This discrepancy is primarily attributed to differences in retrieval wavelengths and fundamental differences between aircraft and satellite observations. AOD generally increases at shorter wavelengths, and since HSRL AOD is retrieved at 532 nm, GEMS AOD may appear lower by comparison. Moreover, HSRL and AERONET provide point-based measurements, while GEMS AOD is averaged over a broader area. When localized high-concentration sources are present, GEMS may report lower values due to spatial averaging.

◎ GK-2B Fused Aerosol Optical Depth

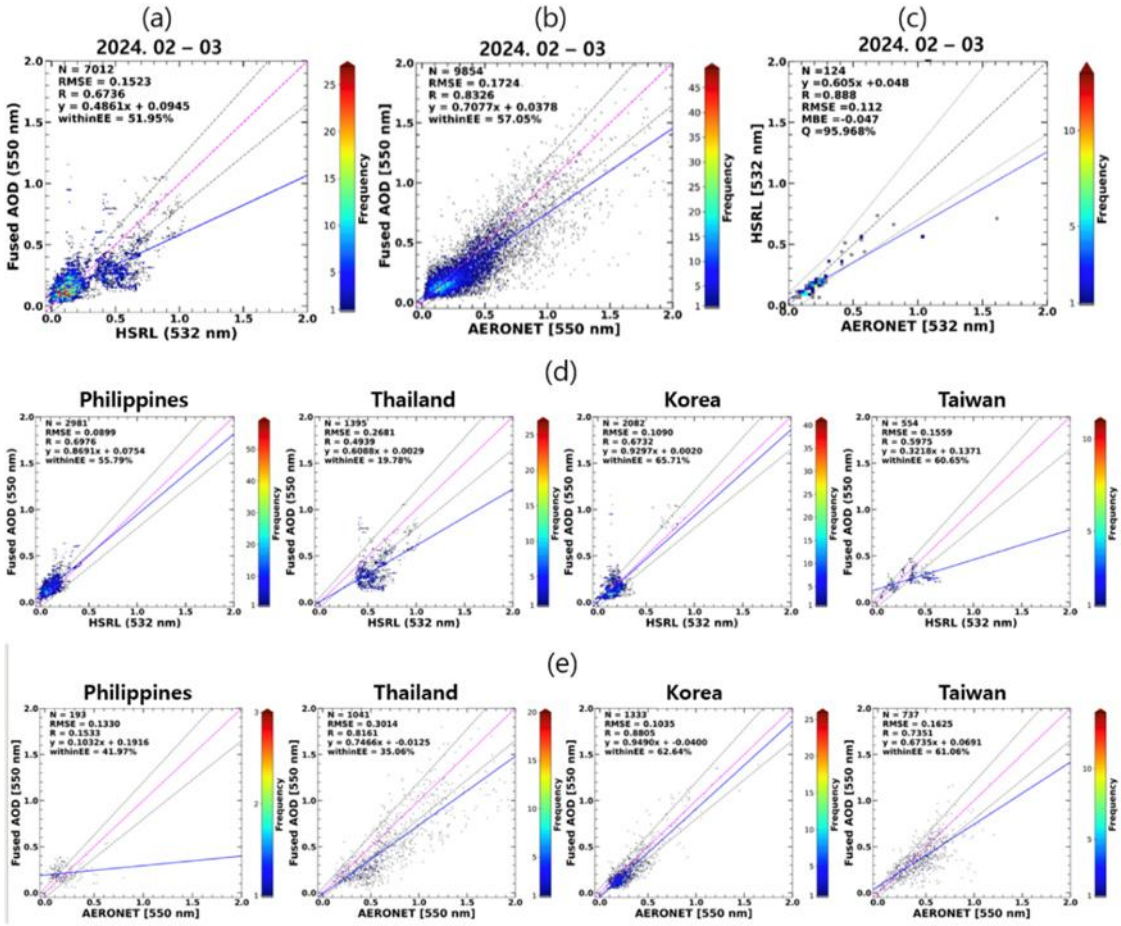

Figure 5-3. (a) Comparison of GK-2B Fused AOD [550 nm] with HSRL AOD [532 nm]; (b) Comparison of GK-2B Fused AOD [550 nm] with AERONET AOD [550 nm]; (c) Comparison of AERONET and HSRL AOD; (d) Country-level validation of Fused AOD against HSRL; (e) Country-level validation of Fused AOD against AERONET. In all scatterplots, the dashed line with wide spacing indicates the 1:1 line (y = x), and the dashed lines with narrow spacing represent the larger of ±0.1 or ±30% as the error margin. The “withinEE” expression denotes the fraction of data points falling inside this error margin.

The GK-2B Fused AOD product (Kim et al., 2024), derived by combining AOD retrievals from GEMS, AMI, and GOCI-II, utilizes a deep neural network (DNN) algorithm designed to compensate for individual limitations of each sensor while maximizing the benefits of fusion. The Fused AOD showed strong performance even in the Philippines when validated against HSRL. Because fusion and re gridding introduced pixel loss, the number of collocated points available for cross-validation was relatively limited. As shown in Figure 5-3(d), the correlation coefficient (R) between Fused AOD and HSRL across the four validation regions ranged from 0.49 to 0.70, with particularly reliable validation results observed in South Korea and the Philippines.

◎ Aerosol layer height (ALH, Version 2.1) and Aerosol effective height (AEH, Version 2.1)

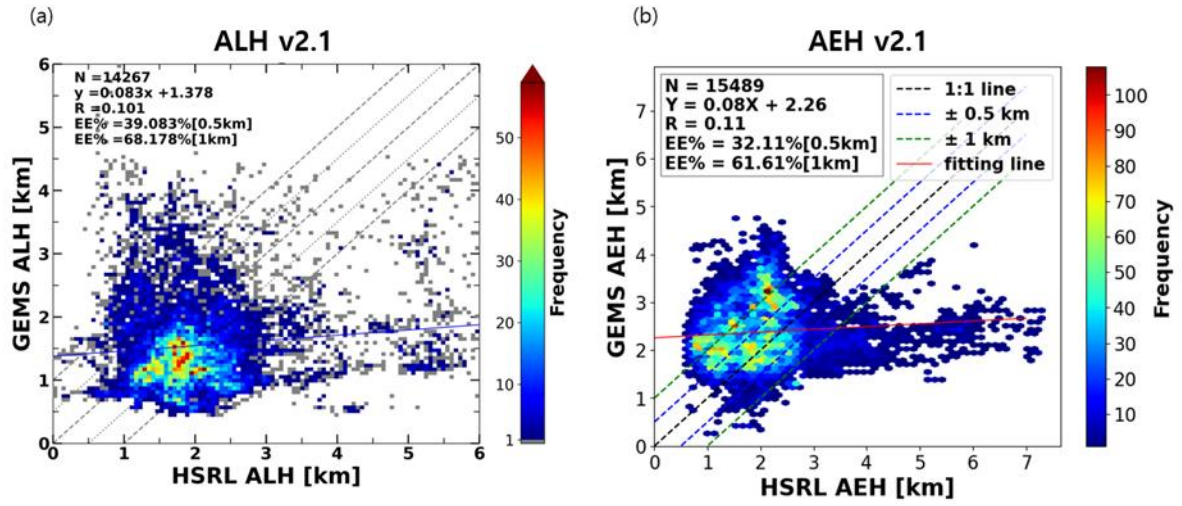

Figure 5-4. (a) Comparison between GEMS ALH and HSRL ALH; (b) Comparison between GEMS AEH and HSRL AEH. For temporal collocation, HSRL measurements within ±30 minutes of the GEMS overpass were averaged. For spatial collocation, GEMS retrievals within a 25 km radius of the HSRL observation pixel were averaged. Each matched ALH (or AEH) pair is shown as a scatter point. In both panels, the dashed line denotes the 1:1 reference, ±0.5 km and ±1 km deviations, respectively. The blue line in panel (a) and the red line in panel (b) is the least-squares regression fit. EE% indicates the percentage of collocated pairs within ±0.5 km or ±1 km of the HSRL reference.

Aerosol layer height (ALH) refers to the altitude where the aerosol extinction coefficient reaches its maximum (i.e., the center of the densest aerosol layer) while aerosol effective height (Park et al., 2025) corresponds to the midpoint between the surface and the top of the aerosol layer. The High Spectral Resolution Lidar-2 (HSRL-2), capable of profiling both ozone and aerosols, provides a valuable reference for validating GEMS-derived aerosol layer height. As shown in Figure 5-4(a), 39% and 68% of GEMS ALH retrievals fell within ±0.5 km and ±1.0 km of the HSRL values, respectively, indicating reasonable accuracy.

According to Figure 5-4(b), 32% of GEMS AEH retrievals were within 0.5 km and 62% within 1.0 km of the HSRL AEH values. In general, good agreement was observed in regions with strong aerosol signals, such as biomass burning areas. In contrast, larger discrepancies were observed in regions with low aerosol concentrations or multilayered vertical structures. Additionally, high-altitude aerosol extinction observed in the HSRL profiles may bias AEH estimates, suggesting the need to apply stricter quality control to the significance of HSRL-derived aerosol extinction coefficients (AEC). Overall, GEMS ALH tended to detect the lower portion of the aerosol peak, while AEH corresponded more closely to the upper portion relative to HSRL, highlighting complementary sensitivities of the two products.

◎ Nitrogen dioxide (NO_2, Version 4.0)

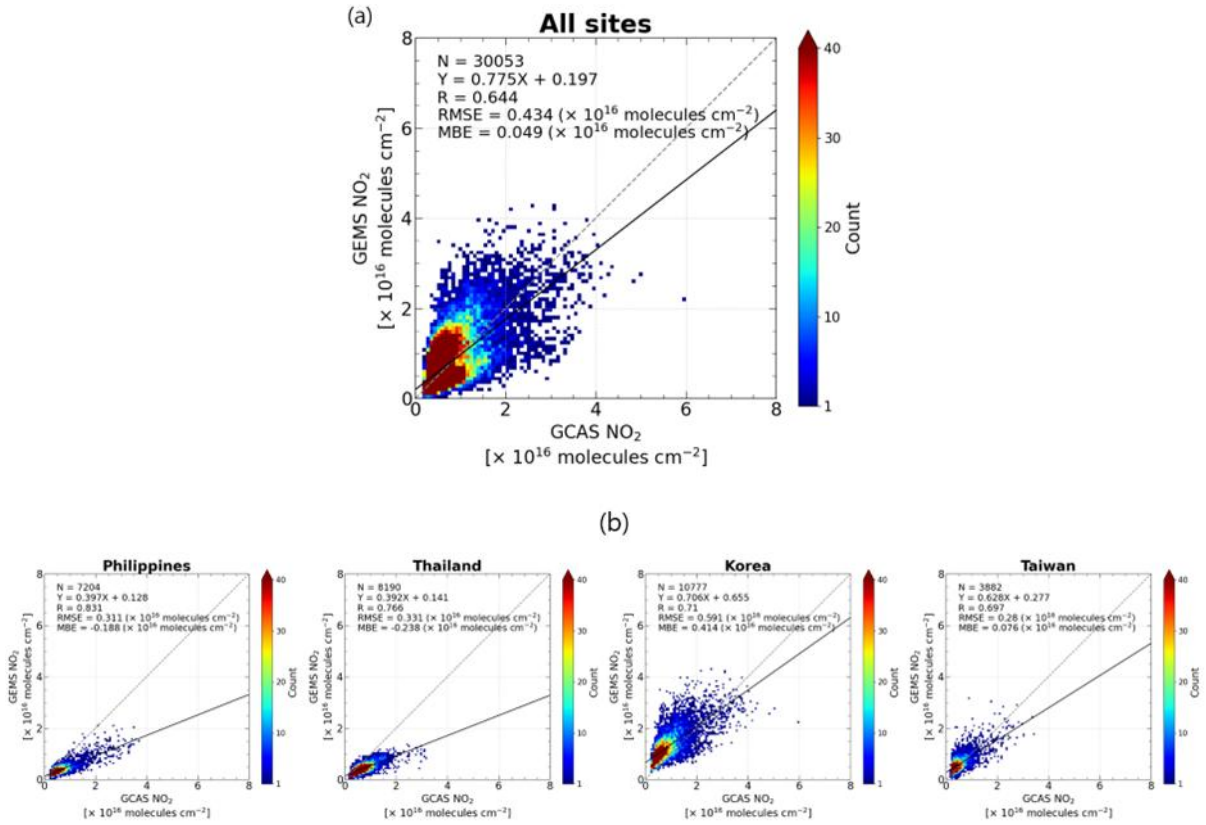

Figure 5-5. (a) Validation of GEMS NO_2 VCD (Version 4.0) against GCAS aircraft observations. (b) Country-level validation results. GCAS NO_2 values were averaged within ±30 minutes of the GEMS overpass time and only when the GCAS roll angle was less than 10°. For spatial collocation, GEMS NO_2 values within a 5 km radius of each GCAS pixel were averaged. The resulting matched pairs are shown as scatterplots.

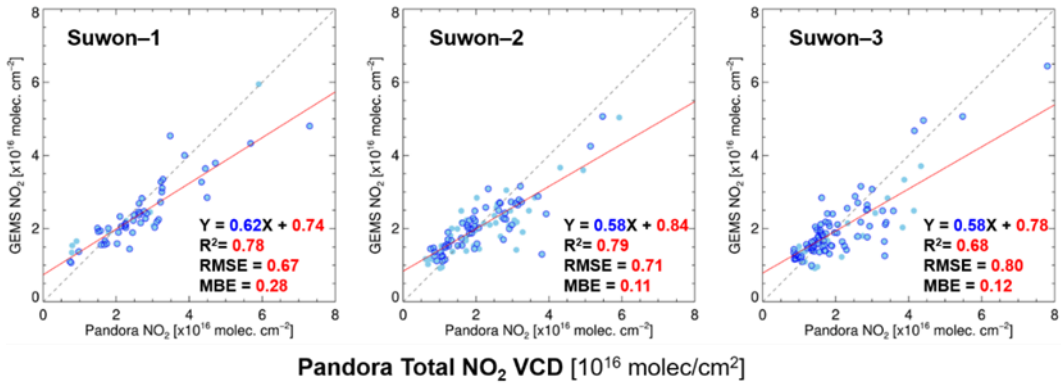

Figure 5-6. Comparison of GEMS NO_2 VCD (Version 4.0) with ground-based Pandora NO_2 VCD observations over Suwon during the ASIA-AQ campaign. The locations of Pandora instruments in Suwon are described in Figure 5-7(b).

Figure 5-5 presents the validation results of GEMS NO_2 (Version 4.0) against NO_2 vertical column densities (VCDs) observed by the GeoCAPE Airborne Simulator (GCAS). In regional comparisons, GEMS NO_2 tended to be underestimated relative to GCAS in the Philippines and Thailand, likely due to frequent cloud cover that limited the quality of satellite retrievals. In contrast, both underestimations and overestimations were observed in Taiwan and South Korea.

To validate the spatial monitoring capacity of GEMS, Pandora spectrometers were densely deployed across the Suwon area during the ASIA-AQ campaign (Figure 5-6). The updated GEMS Level 2 NO_2 product demonstrated significant improvement compared to previous versions. In particular, Version 4.0 reduced the overestimation observed in Version 2.0 by approximately 40%, especially in urban areas. As a result, key validation metrics (including offset, root mean square error (RMSE), and mean bias error (MBE)) were notably improved.

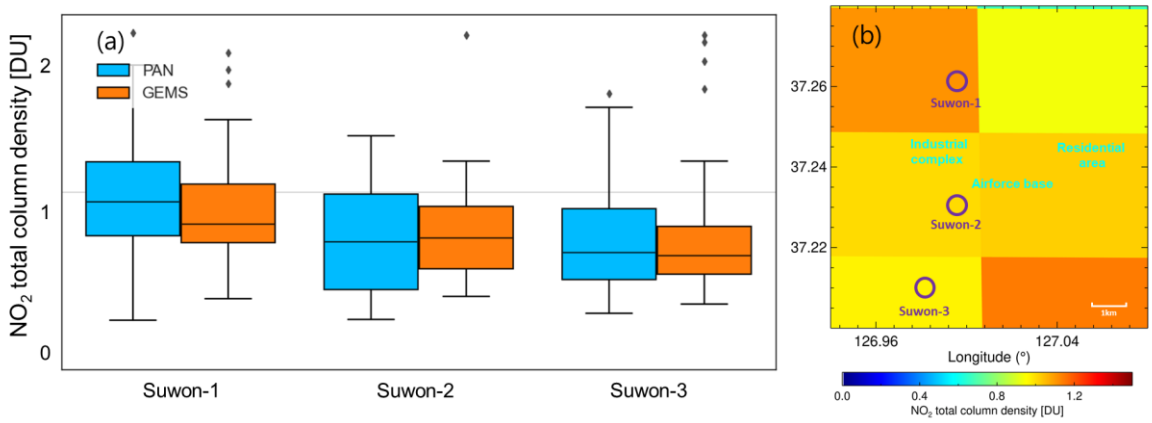

Figure 5-7. (a) Box plots comparing NO_2 vertical column densities from three Pandora instruments and corresponding GEMS pixels in Suwon. (b) Locations of Pandora instruments (circles) within GEMS pixels on January 25, 2024. DU = Dobson Unit.

Figure 5-7(a) presents box plots comparing total column NO_2 concentrations from GEMS and Pandora at three sites in Suwon, highlighting pixel-level variability in the satellite retrievals. Figure 5-7(b) shows the spatial distribution of GEMS pixels and Pandora instrument locations (indicated by circles) on January 25, 2024.

During the campaign, both GEMS and ground-based Pandora observations consistently reported the highest average NO_2 concentrations at Suwon-1 (37.26°N, 126.99°E), with statistical significance at the 95% confidence level, while Suwon-3 (37.21°N, 126.98°E) showed the lowest concentrations. Suwon-1 also exhibited the largest variability in NO_2 concentrations across both datasets. These results demonstrate strong agreement between GEMS and ground-based measurements at the pixel level, indicating that GEMS can

effectively resolve localized pollution and detect spatial variability in NO_2 concentrations at the resolution of its satellite pixels.

◎ Sulfur dioxide (SO_2, Version 2.1)

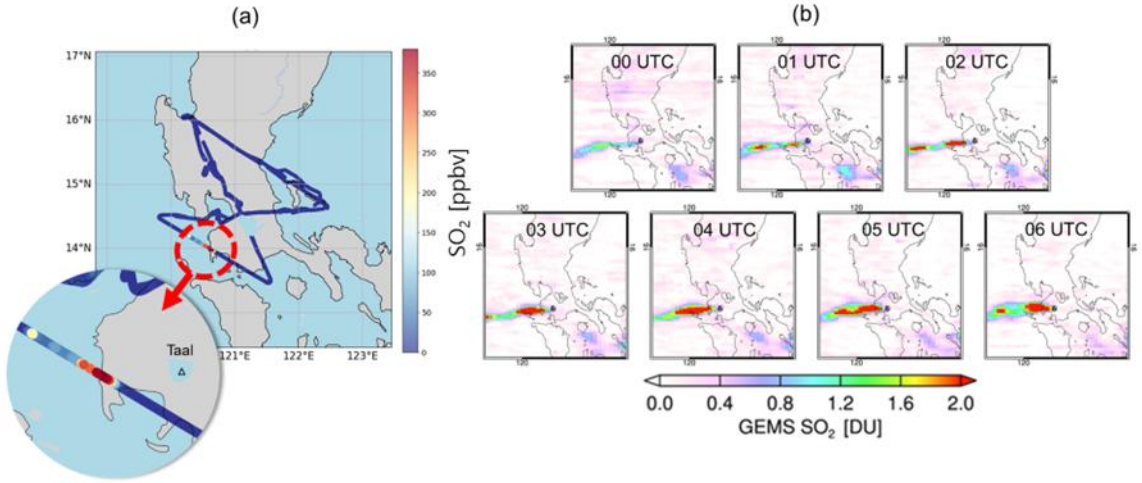

Figure 5-8. (a) Spatial distribution of SO_2 [ppb] observed by the DC-8 aircraft over the Philippines on February 7, 2024; (b) Hourly spatial distribution of SO_2 [DU] retrieved from GEMS. The location of Taal volcano is shown in panel (a).

Figure 5-8 shows the spatial distribution of SO_2 observed on February 7, 2024, over the Philippines from two different platforms: (a) aircraft-based observations from the DC-8 and (b) satellite-based retrievals from GEMS (Version 3.0). The comparison reveals strong consistency between the two datasets. Elevated SO_2 concentrations near latitude 14°N, clearly detected by the DC-8, were also captured by GEMS and are attributed to the high-concentration SO2 plume emitted by the Taal volcano, about 70 km south of Manila. During the observation period, the prevailing easterly winds transported the volcanic plume westward away from Manila, resulting in the downwind interception of the plume as shown in Figure 5-8a. The GEMS observations accurately represented the emission and dispersion of volcanic gases in the region, as confirmed through comparison with other remote sensing datasets.

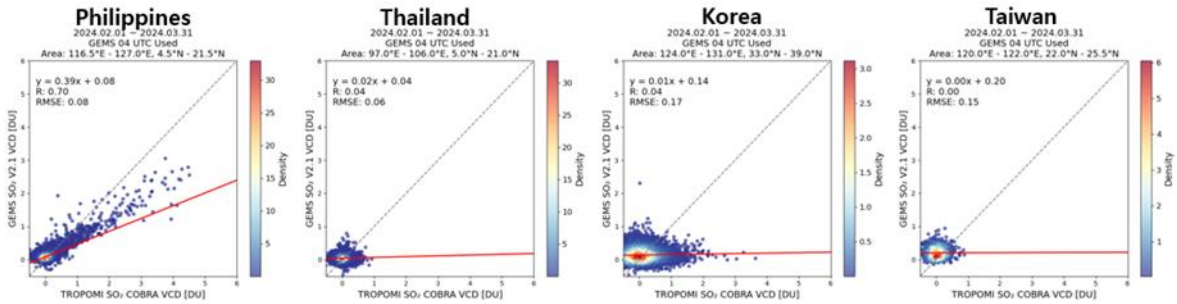

Figure 5-9. Comparison of GEMS SO_2 v3.0 [DU] and TROPOMI SO_2 [DU] data over the Philippines, Thailand, South Korea, and Taiwan. Only the 04:45 UTC GEMS data were used, in order to match the TROPOMI overpass time.

The volcanic activity of Taal during the ASIA-AQ campaign served as a valuable case to assess GEMS SO_2 sensitivity under high-concentration conditions. As shown in Figure 5-9, validation results comparing GEMS and TROPOMI SO_2 indicated the highest agreement in the Philippines. This is likely due to the elevated SO_2 levels from volcanic emissions. In contrast, the other three countries exhibited lower SO2 concentrations, which may have resulted in larger relative retrieval uncertainties. In particular for Korea, the uncertainty is further exacerbated by the inherently lower sensitivity of GEMS to SO_2 within the planetary boundary layer.

◎ Total Ozone (O_3T, Version 2.1)

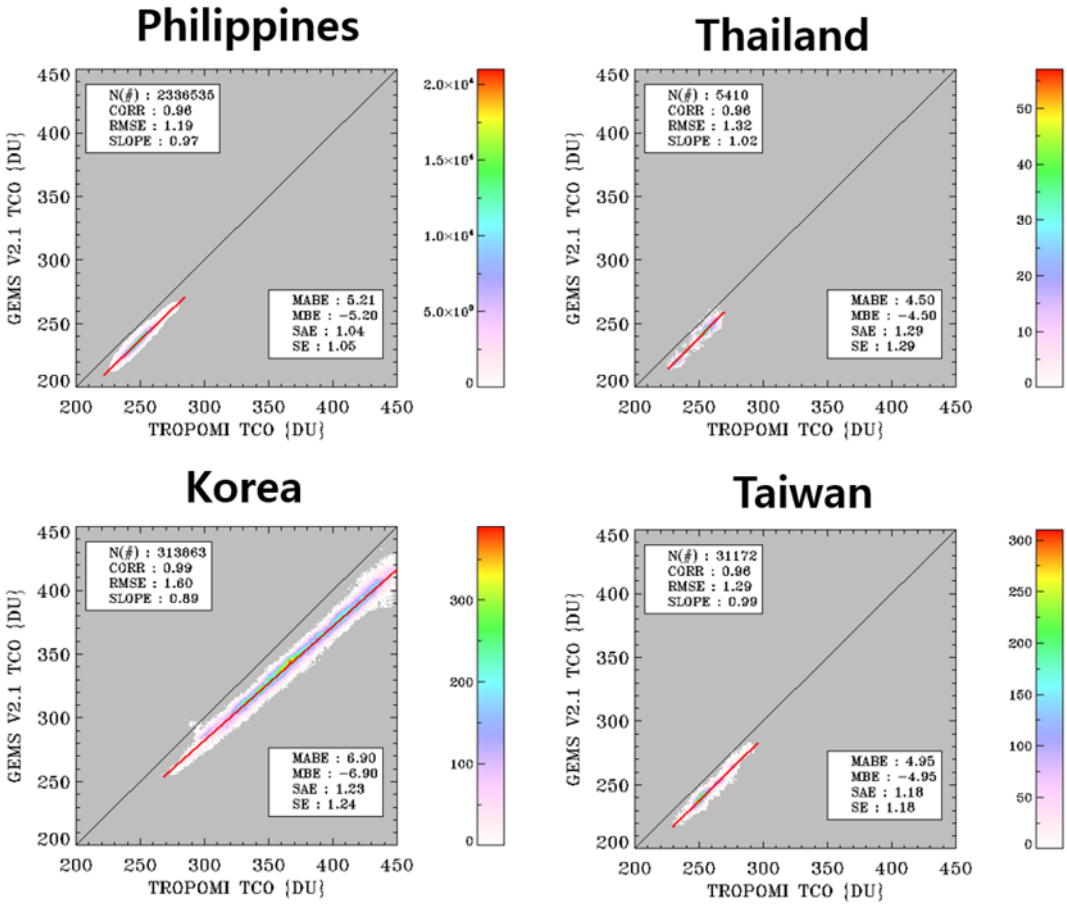

Figure 5-10. Country-level validation of GEMS O_3T (total column ozone, TCO) V2.1 [DU] against TROPOMI [DU]. The dashed line denotes the 1:1 reference. CORR represents the Pearson correlation coefficient. MABE (mean absolute bias error), SAE (standard absolute error), RMSE (root-mean-square error), and SE (standard error) are displayed within the figure.

In this section, total column ozone is abbreviated as TCO, which is the commonly used term in the ozone research and application communities. In contrast, O_3T is the official product name used in the GEMS retrieval system. Throughout this section, O_3T and TCO refer to the same physical quantity, namely the total column amount of ozone expressed in Dobson Units (DU).For total ozone (O_3T), the GEMS O_3T Version 2.1 product was validated using ozone retrievals from the TROPOspheric Monitoring Instrument (TROPOMI) onboard the Sentinel-5P satellite. According to the validation results in figure 5-10, GEMS and TROPOMI total ozone values showed very high correlation (R = 0.96–0.99) and consistent spatial patterns. However, GEMS ozone values were slightly lower than those from Pandora. This underestimation is likely due to GEMS's use of longer UV wavelengths compared to TROPOMI, resulting in reduced sensitivity to stratospheric ozone.

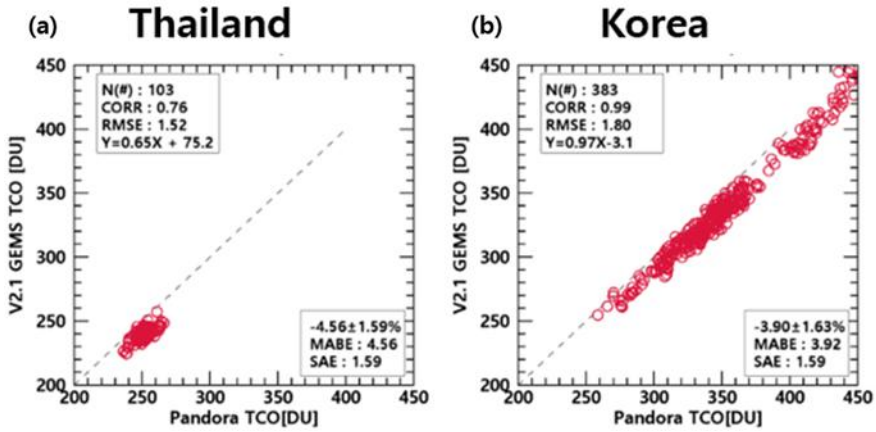

Figure 5-11. Validation of GEMS O_3T (total column ozone, TCO) V2.1 [DU] against Pandora total ozone [DU] in (a) Thailand and (b) South Korea. Pandora observations were available only in these two countries during the ASIA-AQ campaign. The dashed line denotes the 1:1 reference. CORR represents the Pearson correlation coefficient. MABE (mean absolute bias error), SAE (standard absolute error), RMSE (root-mean-square error) are displayed within the figure.

During the ASIA-AQ campaign, Pandora data were available only in Thailand and South Korea (Figure 5-11). As shown in Figure 5-10, the correlation between GEMS and Pandora total column ozone (TCO) observations was very high in South Korea (R = 0.99), whereas in Thailand, a good but lower agreement (R = 0.76) and slight underestimation were observed. Here, R denotes the Pearson correlation coefficient, which corresponds to CORR in the figure annotations.

◎ Ozone profile (O_3P, Version 3.0)

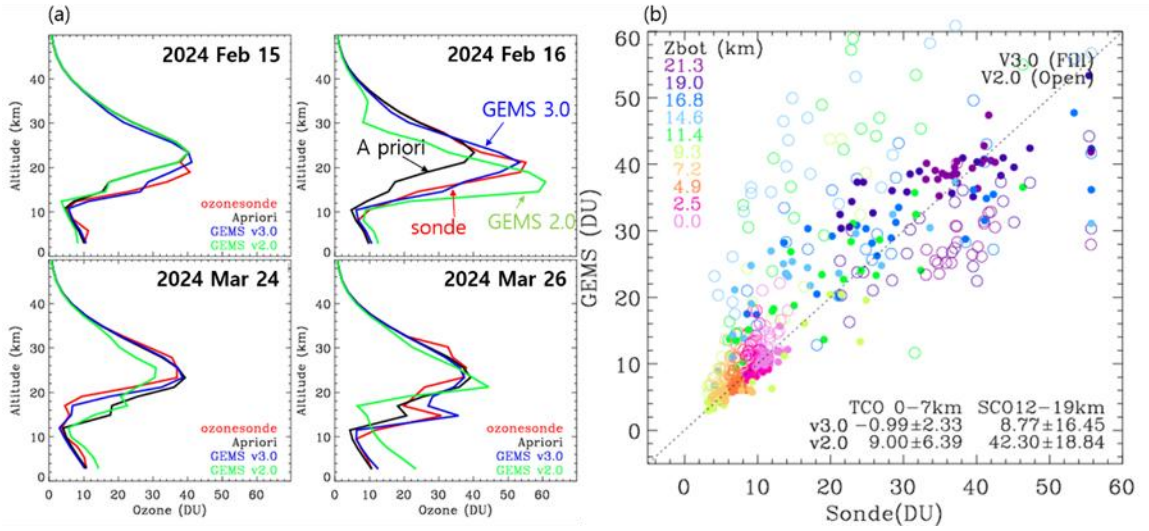

Figure 5-12. (a) Ozone profiles observed by ozonesondes (red) in Seosan and Gongju, compared with GEMS O_3P Version 3.0 (blue), Version 2.0 (light green), and a priori profiles (black); (b) Scatterplot comparing the profile-integrated total column ozonefrom GEMS O_3P Versions 3.0 and 2.0 with ozonesonde observations during the ASIA-AQ campaign. Here, Zbot denotes level height and is indicated by different colors in (b). The tropospheric column ozone (TCO) is calculated by vertically integrating ozone concentrations from 0–7 km and the stratospheric column ozone (SCO) is derived from integration over the 12–19 km altitude range.

The GEMS product of ozone profiles was validated with ozonesonde measurements during the campaign. Figure 5-12a presents a comparison of ozone profiles measured by ozonesondes launched in Seosan and Gongju during February and March, 2024 with GEMS O_3P a priori profiles, GEMS Version 3.0, and GEMS Version 2.0. As shown, GEMS Version 2.0 exhibited a clear tendency to overestimate ozone in the lower stratosphere and underestimate it in the upper stratosphere, particularly overestimating ozone in the lower stratosphere on 16 February and in the lower troposphere on 26 March. In contrast, GEMS Version 3.0 showed improved agreement with ozonesonde profiles and better captured the seasonal variation in the vertical distribution of stratospheric ozone from February to March. The quantitative comparison between GEMS and ozonesonde measurements is presented in Figure 5-12(b) for TCO (Tropospheric Column Ozone, the integrated ozone column from 0 to 7 km) and SCO (Stratospheric Column Ozone, the integrated ozone column from 12 to 19 km). Compared to Version 2.0, which exhibits a substantial positive bias (9.00 in TCO and 42.30 in SCO) and high variability (±6.39 in TCO and ±18.84 in SCO), Version 3.0 shows a marked improvement, reducing the bias (−0.99 in TCO and 8.77 in SCO) with lower scatter (±2.33 in TCO and ±16.45 in SCO).

◎ Formaldehyde (HCHO, Version 3.0)

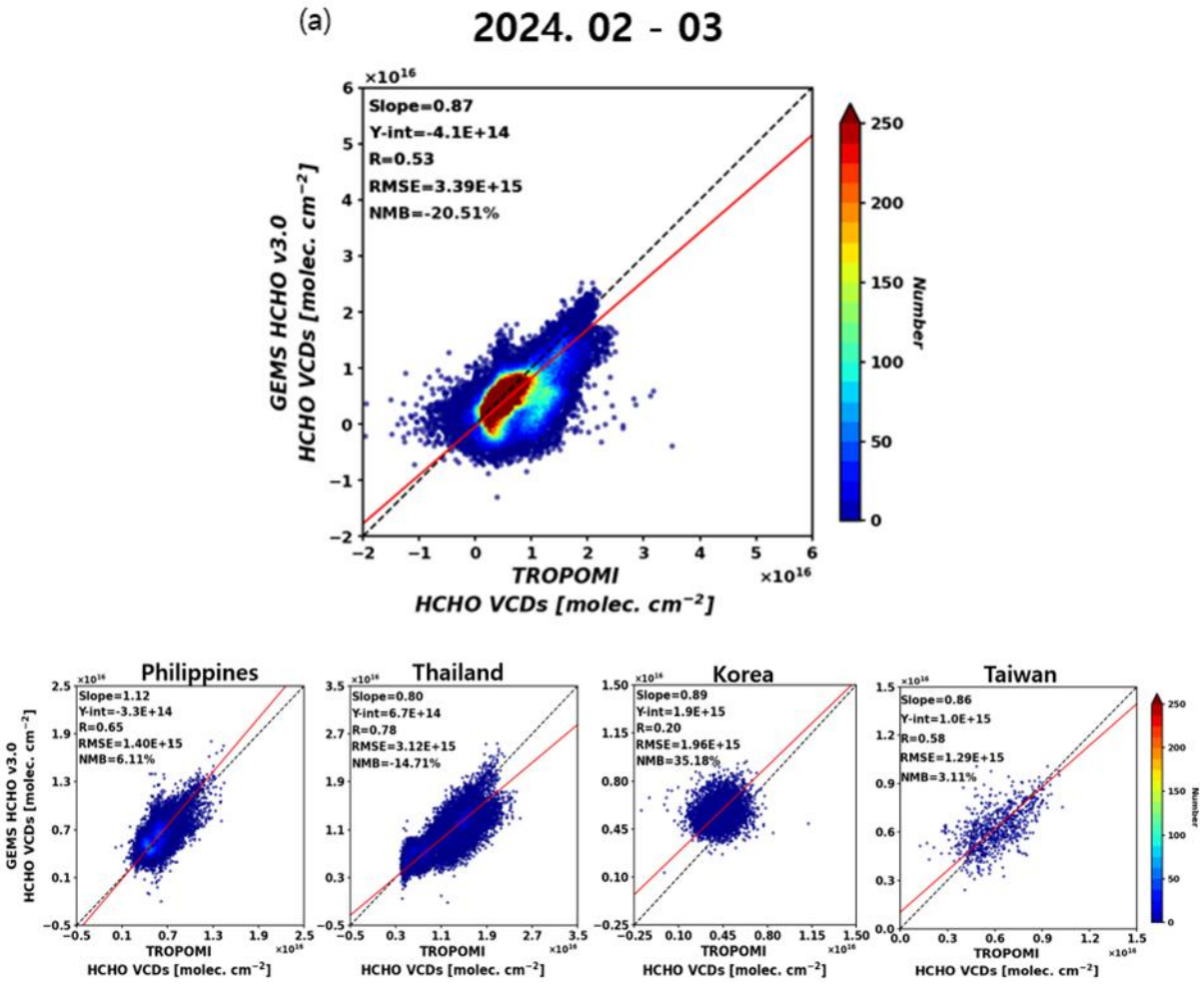

Figure 5-13. (a) Comparison of average GEMS HCHO (Version 3.0) and TROPOMI HCHO vertical column densities (VCDs) over four countries during February–March 2024; (b) Country-level comparison between GEMS and TROPOMI HCHO VCDs. NMB (normalized mean bias), RMSE (Root mean square error) and R are denoted over all collocated pairs. All metrics are computed using temporally and spatially collocated GEMS and TROPOMI VCDs.

Figure 5-13 presents a comparison between GEMS and TROPOMI HCHO vertical column densities (VCDs), averaged over February–March 2024, for the four countries observed during the ASIA-AQ campaign. Across the entire domain, the correlation coefficient (R) between GEMS and TROPOMI was 0.53, though with a range of 0.20 to 0.78. In Southeast Asian regions such as Thailand, Taiwan, and the Philippines, the correlation exceeded 0.58, and the spatial patterns over high-concentration areas were closely aligned between the two products. In contrast, South Korea exhibited lower correlation and higher normalized mean bias (NMB), likely due to low wintertime HCHO concentrations over the Korean Peninsula, which increased the retrieval uncertainty of slant column densities (SCDs) in both TROPOMI and GEMS.

◎ Glyoxal (CHOCHO, Version 2.1)

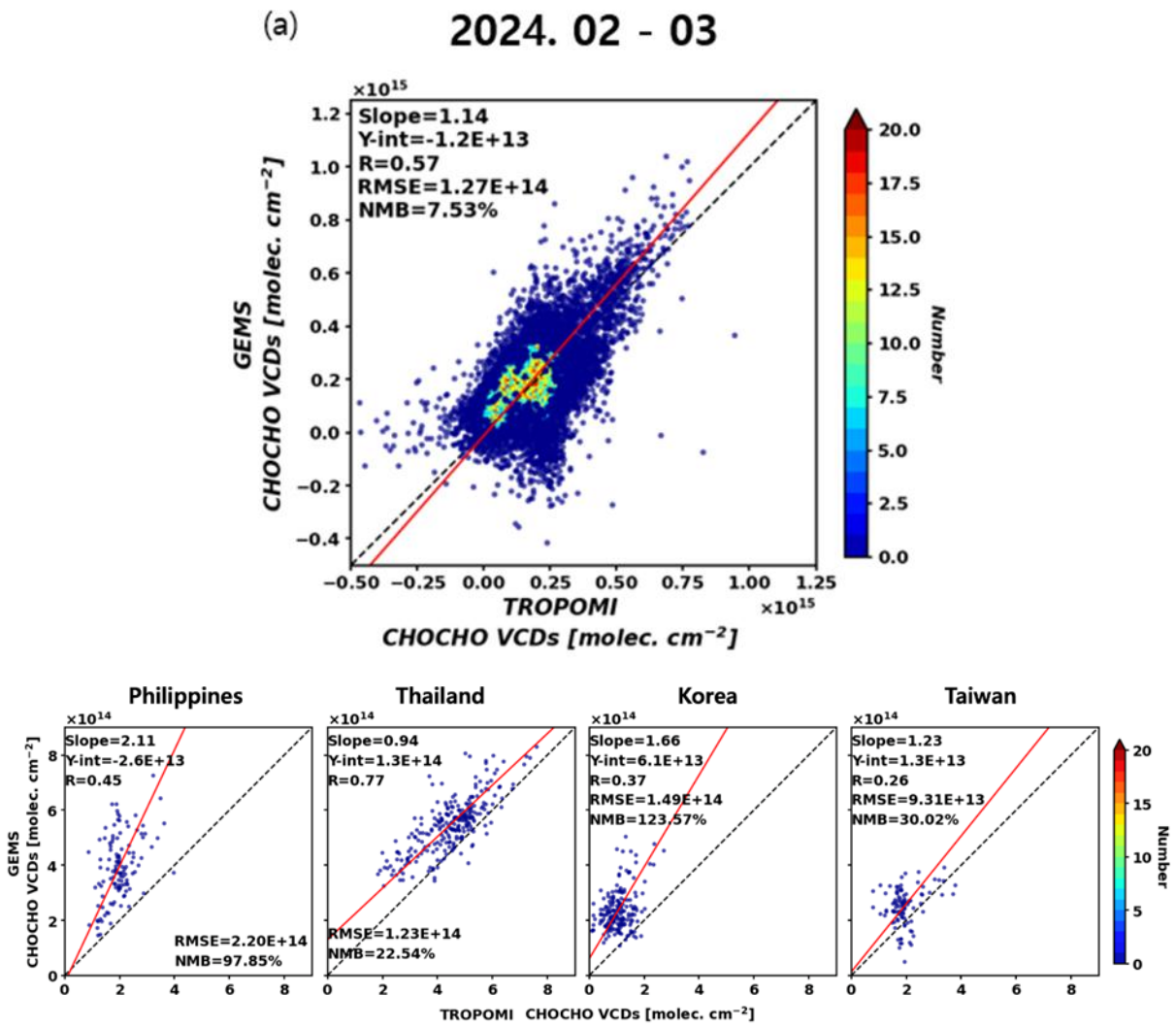

Figure 5-14. (a) Comparison between GEMS CHOCHO (Version 2.1) and TROPOMI CHOCHO VCDs averaged over February–March 2024; (b) Country-level comparison of GEMS and TROPOMI CHOCHO VCDs.

Figure 5-14 presents regional comparisons of GEMS CHOCHO retrievals with TROPOMI. The correlation coefficients by country were as follows: Philippines (0.45), Thailand (0.77), South Korea (0.37), and Taiwan (0.26). Due to lower values in the western part of the domain, the domain-wide mean of GEMS CHOCHO VCDs was 8% higher than TROPOMI (as indicated by the normalized mean bias, NMB). However, over the ASIA-AQ focus regions, GEMS VCDs were substantially higher than TROPOMI values: approximately 23–30% higher over Thailand and Taiwan, and 90–124% higher over the Philippines and South Korea.

Future Research Directions and the Importance of Aircraft Observations

In atmospheric pollution research, aircraft observations serve as an essential tool for providing information on vertical structures of the atmosphere that cannot be captured by surface measurements or satellite column-integrated data. The ASIA-AQ campaign reaffirmed the critical role of aircraft measurements and played a key role in collecting vertical profile data for various air pollutants. In particular, aircraft observations allow for direct in-situ measurements of chemical species and concentrations at specific altitudes, enabling detailed detection of altitude-dependent pollutant variability that satellites may not resolve. Furthermore, aircraft data served as a bridge between ground-based and satellite observations, contributing significantly to the validation and improvement of GEMS satellite products.

While GEMS provides a powerful platform for real-time air pollution monitoring across East Asia, systematic and regular validation through aircraft observations remains essential for ensuring the reliability of its satellite retrievals. Except for stratospheric species such as O_3 and NO_2 and special cases such as volcanic SO_2 or dust-related aerosol plumes, most of the pollutants retrieved by GEMS originate near the surface and are influenced by complex processes involving emission, chemical transformation, and atmospheric transport. These factors introduce uncertainty into the vertical distribution of trace gases, which, if not accurately characterized, can lead to retrieval bias. Therefore, consistent vertical profile comparisons and the development of long-term aircraft-based datasets are vital for reducing uncertainties in satellite retrievals. The aircraft data collected during ASIA-AQ contributed to the assessment of potential biases in GEMS retrievals and helped refine satellite-based concentration estimates.

Current results show that the a priori vertical profile inputs used in the GEMS retrievals of HONO, HCHO, and CHOCHO differ significantly from aircraft observations. A priori profiles play a central role in minimizing retrieval uncertainty and ensuring algorithm stability, with the goal of producing accurate air mass factors (AMFs). Although retrieval developers select optimal a priori profiles based on chemical transport models (CTMs), there is an inherent mismatch between model-derived inputs and aircraft-based direct measurements.

Considering these differences, recalculating AMFs using aircraft-based vertical profiles can produce values that more accurately reflect real atmospheric conditions. In cases where there is a substantial discrepancy between the a priori profiles and aircraft observations, deriving AMFs from measured vertical profiles can serve as a valuable approach for evaluating and improving current GEMS AMFs. This would enhance the accuracy of AMF calculations and contribute to improving the reliability of satellite-derived air quality products. Therefore, it is essential to systematically validate and refine the a priori profiles used in the GEMS retrieval algorithm using the vertical gas profiles obtained from the ASIA-AQ campaign. In addition, various other issues have been identified that affect the validation of satellite observations using aircraft data. These include uncertainties in the calibration and correction status of GEMS Level 1 data, known seasonal variations in solar irradiance, ongoing degradation of UV channel performance, increasing dark current, inadequate correction of stray light, lack of usable

information below 310 nm, the resulting performance degradation in Level 2 products, and unresolved algorithm-specific issues.

Future research should focus on resolving these technical challenges to further enhance GEMS's air quality monitoring capabilities and reduce uncertainty in its data products. Through large-scale, coordinated efforts involving aircraft, ground-based, and modeling systems, the accuracy of GEMS retrievals can be continuously improved. Ultimately, these efforts are expected to strengthen air quality research and support evidence-based policy development across Asia.

4. Policy Recommendations

1. Policy Recommendations for Improving Air Quality in South Korea

The ASIA-AQ campaign reaffirmed several key scientific findings relevant to South Korea's air quality policy: (1) secondary formation (particularly SIA) accounts for the overwhelming majority of domestic $PM_{2.5}$; (2) Controlling NO_x is one of the most critical strategies for reducing secondary $PM_{2.5}$ formation; and (3) VOCs, including aromatic species such as toluene, contribute to wintertime $PM_{2.5}$ formation and also play a role in high ozone episodes during spring and summer.

These conclusions are consistent with findings from the 2016 KORUS-AQ campaign. The fact that similar policy implications remain valid nearly eight years later suggests that, even in 2025, NO_x and VOC reduction must remain central pillars of South Korea's air quality strategy. The Third Comprehensive Air Quality Improvement Plan (2023–2032) sets national reduction targets of approximately 45% for NO_x and 12% for VOCs relative to 2021 levels. These targets must be fully realized. While substantial reductions have already been achieved in the industrial and transportation sectors, further progress is required in heavy industries such as cement, steel, and petrochemicals.

As emphasized in both ASIA-AQ and KORUS-AQ, VOC reduction is essential for controlling both $PM_{2.5}$ and ozone. However, the current VOC reduction target of 12% remains insufficient given its importance. This limitation is largely due to the lack of species-resolved VOC emission inventories, which impedes the development of sector-specific control strategies. Therefore, the government's ongoing efforts to improve VOC inventories through detailed species- and sector-level measurements, and to develop corresponding emission reduction technologies, must be urgently advanced. Positive Matrix Factorization (PMF) source apportionment analysis of VOCs is ongoing and helps obtain information about species-resolved VOC emissions. Achieving significant reductions in $PM_{2.5}$ and ozone concentrations will require not only continued NO_x control but also strengthened and proactive VOC control measures.

The ASIA-AQ campaign also included an isotopic analysis of carbon in Seoul, which confirmed a clear fossil fuel signature in the air pollution profile. Despite improvements in air quality driven by the expansion of eco-friendly transportation, fossil fuel combustion (particularly from diesel vehicles) continues to pose significant health risks in Seoul and other metropolitan areas. This highlights the need to accelerate the adoption of eco-friendly or zero-emission vehicles in alignment with the national carbon neutrality roadmap. Policies such as the early retirement of Grade 4 diesel vehicles should deliver measurable outcomes, and further studies are needed to quantify their impacts.

Despite being conducted during a high-pollution season, the ASIA-AQ campaign observed substantially lower $PM_{2.5}$ levels compared to the same season from 2015 to 2023. In addition, compared to KORUS-AQ, the ASIA-AQ campaign provided clear evidence of the significant influences of regional anthropogenic emission reductions, meteorological variability, and

transboundary pollution on observed $PM_{2.5}$ concentrations during Korea's seasonal air quality management periods.

The campaign also demonstrated improvements in modeling and data assimilation performance using satellite data from GEMS. The enhanced quality of satellite-derived products, combined with progress in international validation efforts, highlights the importance of continued investment in satellite-based environmental monitoring. International cooperation for validation and satellite data quality assurance must be sustained to fully realize the potential of satellite systems in forecasting, evaluating, and managing air quality in the 2020s and beyond.

2. Policy Recommendations for Improving Air Quality in Seoul

Based on the findings from the ASIA-AQ campaign, this section outlines policy recommendations and project concepts that can be effectively integrated with Seoul's ongoing air quality improvement initiatives. These recommendations aim to enhance the effectiveness of current measures (such as the seasonal PM management program, emissions controls for industrial facilities, and VOC reduction strategies) through improved linkage and coordination.

Analysis of observation data from ASIA-AQ showed that more than 80% of wintertime $PM_{2.5}$ episodes in Seoul were attributed to secondary formation, with inorganic nitrate accounting for the largest share. Therefore, reducing NO_x emissions, particularly from mobile sources, is essential. Seoul is already implementing policies to restrict older diesel vehicles and promote the adoption of low-emission vehicles. These efforts should be expanded through stricter restrictions on Grade 5 vehicles and further expansion of Green Transportation Zones. In parallel, the city should accelerate the adoption of electric and hydrogen vehicles, expand charging infrastructure, and promote alternatives to private vehicle use through improved public transit, walking, and cycling infrastructure.

To reduce NO_x from stationary combustion sources, Seoul should continue promoting the replacement of outdated boilers with low-NO_x burners and eco-friendly systems, and support improvements in combustion efficiency to further reduce emissions. The formation of nitrate particles is also strongly influenced by NH_3. While urban areas such as Seoul have few traditional agricultural NH_3 sources, unexpected sources exist, including water treatment facilities, landfills, and diesel exhaust fluid (DEF) systems. Accurate identification and continuous monitoring of urban ammonia sources are therefore needed, along with the establishment of a real-time monitoring system. Furthermore, ammonia transported from neighboring municipalities may also contribute to nitrate formation in Seoul, requiring inter-regional coordination and joint response measures.

Ensuring the long-term sustainability of $PM_{2.5}$ reduction requires improved control of VOCs. VOCs contribute to the formation of SOA and also influence summertime ozone concentrations. ASIA-AQ findings confirmed that specific VOCs (such as toluene) are major

precursors to SOA. Accordingly, Seoul should adopt stricter regulations on VOCs from consumer products and industrial sources, in line with international best practices. VOC content standards for consumer products should be strengthened, and the use of low-VOC alternatives should be actively encouraged. Emissions from small-scale businesses (such as auto body shops and print shops) should be managed through the adoption of best available control technologies (BACT). Regional collaboration is also needed to manage high concentrations of VOCs entering Seoul from nearby industrial complexes. Expanding the current pilot ozone season management program to a nationwide scale may also be effective. In addition, VOC control should be incorporated into the winter PM seasonal management framework to enable year-round integrated pollution management.

To support effective $PM_{2.5}$ reduction policies, a detailed and continuously updated emissions database is essential. Seoul should establish a city-specific inventory of precursor emissions (NO_x, VOCs, NH_3), reflecting the characteristics of local sources. Activity data and emission factors must be improved through regular field surveys, and real-time monitoring of major emission sources should be enhanced to ensure timely data updates. This database should also support scenario-based policy simulations to enable evidence-based decision-making.

Citizen participation and communication are critical to the success of air quality policies. A real-time air quality forecasting and alert system should be developed to provide the public with timely and customized health advisories based on individual health conditions and lifestyle factors. Public understanding and engagement should also be promoted through open access to air quality research campaigns and integration with environmental education programs. Establishing a feedback loop among researchers, policymakers, and citizens will support the development and implementation of more effective and responsive air quality policies.

References

Adachi, K., Zaizen, Y., Kajino, M., and Igarashi, Y.: Mixing state of regionally transported soot particles and the coating effect on their size and shape at a mountain site in Japan, Journal of Geophysical Research: Atmospheres, 119, 5386–5396, 10.1002/2013jd020880, 2014.

Cho, Y., Kim, J., Go, S., Kim, M., Lee, S., Kim, M., Chong, H., Lee, W.-J., Lee, D.-W., Torres, O., and Park, S. S.: First atmospheric aerosol-monitoring results from the Geostationary Environment Monitoring Spectrometer (GEMS) over Asia, Atmospheric Measurement Techniques, 17, 4369–4390, 10.5194/amt-17-4369-2024, 2024.

Faulkner, W. B. and Shaw, B. W.: Review of ammonia emission factors for United States animal agriculture, Atmospheric Environment, 42, 6567–6574, 10.1016/j.atmosenv.2008.04.021, 2008.

Grosjean, D. and Seinfeld, J. H.: Parameterization of the formation potential of secondary organic aerosols, Atmospheric Environment (1967), 23, 1733–1747, 10.1016/0004-6981(89)90058-9, 1989.

Kim, J., Lee, J., Yun, C., Lee, M., Lee, H., Kim, K., Lee, H. S., Chang, L., and Lee, G.: Nocturnal N2O5 and NO3 chemistry and its impact on wintertime HNO3 in Seoul during ASIA-AQ campaign, Atmospheric Environment, 365, 10.1016/j.atmosenv.2025.121698, 2026.

Kim, M., Kim, J., Lim, H., Lee, S., Cho, Y., Lee, Y.-G., Go, S., and Lee, K.: Aerosol optical depth data fusion with Geostationary Korea Multi-Purpose Satellite (GEO-KOMPSAT-2) instruments GEMS, AMI, and GOCI-II: statistical and deep neural network methods, Atmospheric Measurement Techniques, 17, 4317–4335, 10.5194/amt-17-4317-2024, 2024.

Lee, H., Lee, M., Lim, S., Chang, L., Kim, K., Choi, Y., Park, M., Gil, J., Kim, J. A., and Yun, C.: PM2.5 nitrate formation during winter haze episodes: insights from Seoul, South Korea., Environmental Science: Processes and Impacts, under review.

Lee, S., Kim, M., Kim, S. Y., Lee, D. W., Lee, H., Kim, J., Le, S., and Liu, Y.: Assessment of long-range transboundary aerosols in Seoul, South Korea from Geostationary Ocean Color Imager (GOCI) and ground-based observations, Environ Pollut, 269, 115924, 10.1016/j.envpol.2020.115924, 2021.

Lee, S., Kim, J., Choi, M., Hong, J., Lim, H., Eck, T. F., Holben, B. N., Ahn, J. Y., Kim, J., and Koo, J. H.: Analysis of long-range transboundary transport (LRTT) effect on Korean aerosol pollution during the KORUS-AQ campaign, Atmospheric Environment, 204, 53–67, 10.1016/j.atmosenv.2019.02.020, 2019.

Lim, S., Lee, M., and Yoo, H. J.: Size distributions, mixing state, and morphology of refractory black carbon in an urban atmosphere of northeast Asia during summer, Sci Total Environ, 856, 158436, 10.1016/j.scitotenv.2022.158436, 2023.

Lim, S., Lee, M., Laj, P., Kim, S.-W., Ahn, K.-H., Gil, J., Shang, X., Zanatta, M., and Kang, K.-S.: Regional characteristics of fine aerosol mass increase elucidated from long-term observations and KORUS-AQ campaign at a Northeast Asian background site, Elementa: Science of the Anthropocene, 10, 10.1525/elementa.2022.00020, 2022.

Lim, S., Bae, M.-S., Jang, J., Dwivedi, A. K., Gil, J., Kim, J. a., Lee, M., Oh, S.-H., Shin, S.-A., and Chang, L.-S.: Exploring fine-aerosol episodes in urban Seoul during the cold season of the 2021 SIJAQ campaign: Measurement evidences of heterogeneous reactions on black carbon particles, Atmospheric Environment, 342, 10.1016/j.atmosenv.2024.120926, 2025.

Nault, B. A., Campuzano-Jost, P., Day, D. A., Schroder, J. C., Anderson, B., Beyersdorf, A. J., Blake, D. R., Brune, W. H., Choi, Y., Corr, C. A., de Gouw, J. A., Dibb, J., DiGangi, J. P., Diskin, G. S., Fried, A., Huey, L. G., Kim, M. J., Knote, C. J., Lamb, K. D., Lee, T., Park, T., Pusede, S. E., Scheuer, E., Thornhill, K. L., Woo, J.-H., and Jimenez, J. L.: Secondary organic aerosol production from local emissions dominates the organic aerosol budget over Seoul, South Korea, during KORUS-AQ, Atmospheric Chemistry and Physics, 18, 17769–17800, 10.5194/acp-18-17769-2018, 2018.

Park, S. S., Kim, J., Cho, Y., Lee, H., Park, J., Lee, D.-W., Lee, W.-J., and Kim, D.-R.: Retrieval algorithm for aerosol effective height from the Geostationary Environment Monitoring Spectrometer (GEMS), Atmospheric Measurement Techniques, 18, 2241–2259, 10.5194/amt-18-2241-2025, 2025.

Xu, Z., Liu, M., Zhang, M., Song, Y., Wang, S., Zhang, L., Xu, T., Wang, T., Yan, C., Zhou, T., Sun, Y., Pan, Y., Hu, M., Zheng, M., and Zhu, T.: High efficiency of livestock ammonia emission controls in alleviating particulate nitrate during a severe winter haze episode in northern China, Atmospheric Chemistry and Physics, 19, 5605–5613, 10.5194/acp-19-5605-2019, 2019.